Charles University in Prague
Faculty of Mathematics and Physics

MASTER THESIS

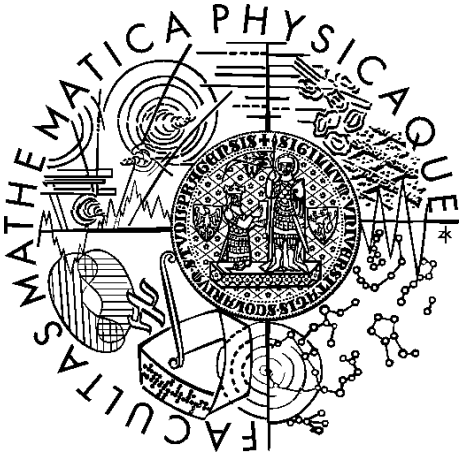

David Paleček

Redox Dependence of Excitation Quenching by Quinones in Bacteriochlorophyll Aggregates

Department of Chemical Physics and Optics

Supervisor of the master thesis: RNDr. Roman Dědic, Ph.D.
Study programme: Physics
Specialization: Biophysics and Chemical Physics

Prague 2011

I want to express my appreciation to my supervisor RNDr. Roman Dědic, PhD. for his constructive help during my experimental work and to Mgr. Jan Alster for preparing samples for my experiments. Special thanks belongs to my family for providing me ideal conditions for my studies at Charles University.

I declare that I carried out this master thesis independently, and only with the cited sources, literature and other professional sources.

I understand that my work relates to the rights and obligations under the Act No. 121/2000 Coll., the Copyright Act, as amended, in particular the fact that the Charles University in Prague has the right to conclude a license agreement on the use of this work as a school work pursuant to Section 60 paragraph 1 of the Copyright Act.

In ..... date ..... Signature

Název práce: Vliv redoxního stavu na zhášení excitace v bakteriochlorofylových agregátech
Autor: David Paleček
Katedra: Katedra chemické fyziky a optiky
Vedoucí diplomové práce: RNDr. Roman Dědic, Ph.D., Katedra chemické fyziky a optiky

Abstrakt: Využitím pouhých 4 % sluneční energie dopadajících na Zemi by bylo možno pokrýt současnou energetickou spotřebu lidstva. Vhodným světlosběrným systémem sloužícím jako inspirace pro vývoj umělé fotosyntézy se zdají být chlorosomy zelených sirných bakterií. V této práci byly porovnány absorpční a hole burningová spektra uměle připravených agregátů podobných chlorosomům s různým složením, s cílem ověřit roli chinonů při zhášení excitace v těchto agregátech a prozkoumat jeho redoxní závislost. Absorpční spektra za pokojové a heliové teploty ukázala na podobnost umělých agregátů s chlorosomy. Hole burnigový experiment potvrdil předpokládanou roli chinonů při zhášení excitace za aerobních podmínek. Na druhou stranu, za anaerobních podmínek bylo pozorováno ještě výraznější zhášení excitace pro některé vlnové délky. Výrazné vylepšení původní aparatury umožnilo získat kvalitnější experimentální data, která nastínila mnoho nových otázek, na které stojí za to se pokusit najít v budoucnu odpovědi.

Klíčová slova: spektrální hole burning, bakteriochlorofylové agregáty, zhášení excitace, chinony

Title: Redox Dependence of Excitation Quenching by Quinones in Bacteriochlorophyll Aggregates
Author: David Paleček
Department: Department of Chemical Physics and Optics
Supervisor: RNDr. Roman Dědic, Ph.D., Department of Chemical Physics and Optics

Abstract: Harvesting only 4 % of light striking the Earth could possibly fulfill present energy demands of a mankind. Chlorosome of green sulfur bacteria is regarded as suitable light-harvesting system for photosynthesis imitation. This work presents comparison of absorption and hole burning spectra of artificially prepared aggregates similar to chlorosomes with different compositions in order to verify the proposed role of quinones in excitation quenching and its redox dependence. Absorption spectra at room and helium temperature showed a resemblance between artificial aggregates and chlorosomes. Hole burning experiments verified the role of quinones in excitation quenching under aerobic conditions. Even more pronounced excitation quenching was observed under anaerobic conditions. Significant improvements of the original experimental set-up provided better experimental data which raised many further question that are worth trying to answer in the future.

Keywords: spectral hole burning, bacteriochlorophyll aggregates, excitation quenching, quinones

Contents

1. Preface

Chlorosomes of green sulfur bacteria represent one of the most effective light-harvesting antennas found in nature at all. They are known for high efficiency of solar quanta capture and for self-aggregating properties with minimal need of protein structure. That enables simple *in vitro* preparation of bacteriochlorophyll *c* (BChl *c*) aggregates, exhibiting similar optical properties to chlorosomes. Basic as well as applied research in nanotechnology and development of artificial photosynthesis are in progress. Artificial photosynthesis is believed to bring forth cheap alternative to silicon-based photovoltaic cells for electric energy production. Photosynthesis is also the only process in nature capable of water and other substrates (with general formula H_2X) oxidation, which is promising for cheap production of hydrogen gas as a clean fuel.

Quinones and carotenoids play an important protection role against oxidative damage due to excess light irradiation of BChl *c* aggregates. These molecules quench excessive excitation energy on a time scale of ps. Therefore, spectral hole burning spectroscopy is suitable method for studying excitation quenching which is proposed to be redox dependent (FRIGAARD et al., 1997, 1998).

Hole burning is an indirect spectroscopic method for studying fast processes in photosynthesis with ability to suppress inhomogeneous broadening of linear absorption and emission spectra. This work presents absorption and hole burning experiments results on BChl *c* aggregates with and without quinones at both aerobic and anaerobic conditions, in order to elucidate the role of quinones in excitation quenching in BChl *c* aggregates. These results are compared with those previously published on aggregates as well as on chlorosomes (PŠENČÍK et al., 1994, 1998; ALSTER et al., 2008)

Presented work was supported by the following projects, MSM 0021620835 from the Ministry of Education, Youth, and Sports of the Czech Republic and GAUK number 113-10/251146. Preliminary results were presented at an international conference 15th International Congress on Photosynthesis, held in Beijing and also at contextual satellite meeting Photosynthetic Light Harvesting in Tianjin, China.

2. Photosynthesis

Principle of photosynthesis is solar energy conversion to the energy of chemical bonds. That mostly happens by subsequent conversion process of solar radiation energy quantum $h\nu$, at first to electrochemical energy by charge separation, consequently to chemical potential of protons μ_{H^+} due to oxidation-reduction reactions, and finally to the energy of anhydride bonds in ATP and redox energy of NADPH utilizing proton gradient. As an electron donor serves in photosynthesis so-called water oxidizing complex (WOC), which produce oxygen as a waste product. One molecule of the oxygen is produced by approximately 2500 chlorophyll molecules (EMERSON – ARNOLD, 1932). This result led to the discovery of chlorophylls organization into photosynthetic units consisting of light-harvesting antennas and reaction centers (RC). Light-harvesting antennas capture photons of solar quanta by excitation of photosynthetic pigments. Excitation in a form of exciton is funneled to the RC, where charge separation and its further stabilization using oxidation-reduction reactions occurs. Such a structure originates in a small photon absorption cross section of chlorophyll and high rate of photochemical reactions in RC. Therefore, without the antenna systems, RC would be inactive for the most of the time. After series of downhill reactions (in terms of redox potential), electron is transferred through the membrane and reduces $NADP^+$ to NADPH. At the same time, proton electrochemical gradient is generated on opposite sides of the photosynthetic membrane as a consequence of electron transfer. Proton transfer back to stromal side of a membrane to equilibrate the proton motive force is possible only through transmembrane protein called ATPase. ATPase utilize the proton motive force for formation of ATP that is macroenergetic molecule which works as an energy source for all living organisms. For instance, human body requires such an amount of ATP a day that equals its own weight (TÖRNROTH-HORSEFIELD – NEUTZE, 2008).

3. Anoxygenic Phototrophic Bacteria

Based on Darwin's evolutionary theory, all living organisms have common ancestor, and therefore, they are related to each other to certain extent. According to this extent of relation one can classify all living organisms on Earth. Suitable method for such classification is based on analysis of small rRNA sequences, which was introduced by Carl Woese (WOESE et al., 1975) who first proposed division to three basic domains of life: bacteria, archea and eukarya (WOESE – FOX, 1977). The theory of this molecular evolution method says that closely related species will contain highly similar macromolecules, while distant relatives will have more diverged structure depending on the time elapsed from their common ancestor occurrence. Degree of difference in macromolecule structure is derived from base sequence differences of nucleic acids which code these macromolecules. Most suitable macromolecule for identifying phylogenetic relations is rRNA because of its universal presence in all organisms. Moreover different parts of rRNA differ in tendency for sequence changes. This property can be used for classification of close and distant relatives utilizing swiftly and slowly changing sequences respectively. The phylogenetic tree based on this molecular evolution method is depicted in figure 3.1

Anoxygenic phototrophic bacteria is a unique group of Eubacteria, predominantly for their ability to perform photosynthesis in anaerobic low light conditions without production of oxygen. Because of these properties and extreme heterogeneity of this group, anoxygenic phototrophic bacteria became important group for studying basic problems of photosynthesis (IMHOFF, 1995), such as optimization of light harvesting antennas (FASSIOLI et al., 2010), excitation energy transfer (SUNDSTRÖM – van GRONDELLE, 1995), pigment-protein complex structures (CAMARA-ARTIGAS et al., 2003; PŠENČÍK et al., 2006, 2010). Despite the great variety in morphological, physiological, and molecular structure properties, we can distinguish according to phenotypes, as mentioned previously, between the green sulfur bacteria, the green non-sulfur bacteria, the purple sulfur bacteria, the purple non-sulfur bacteria, and heliobacteria.

The anaerobic conditions are essential for phototrophic behaviour to the most of the representatives because synthesis of photosynthetic pigments is suppressed by oxygen occurrence. Other common feature to anoxygenic phototrophic bacteria is that they are unable to use water as an electron donor because that would cause oxygen production. They use instead sulfide, other sulfur compounds, hydrogen, and even some small organic molecules (IMHOFF, 1995).

3.1 Green Sulfur Bacteria

Green sulfur bacteria (also called Chlorobi) are characteristic for non-motile and ovoid cells without flagella. On the basis of pigment composition green and brown species of green sulfur bacteria can be distinguished. Green species contain mainly BChl *c*,*d* and carotenoid chlorobactane. On the contrary, brown species contain BChl *e* and carotenoids isorenieratene and β-isorenieratene. Different pigment

content results in different absorption spectra which has an ecological consequence, as the carotenoid content may adapt to grow conditions and abundance in terms of bacteria light spectrum exposure (IMHOFF, 1995). Green species live under a layer of purple sulfur bacteria which filter the light spectrum in a way that available wavelengths for green sulfur bacteria are around 450 nm. That is precisely where chlorobactane absorbs. On the other hand, brown species occur dominantly buried by algae in deep bacterial plates where available wavelengths are between 500 – 550 nm, same as isorenieratene-containing bacteria absorption band (GEMERDEN – MAS, 1995).

Green sulfur bacteria similarly to green non-sulfur bacteria do not contain intracytoplasmic membrane systems. In these bacteria, BChl *c* is almost solitary light-harvesting pigment, which is present in a supramolecular complexes called chlorosomes. They are attached to the cytoplasmic membrane and have very specific and unique properties which are thoroughly discussed in section 3.6. BChl *a* is also present, mainly in reaction centers (RC) and baseplate, which interconnects chlorosomes with the RCs. The green sulfur bacteria has also Fenna-Matthews-Olson (FMO) complex which contain BChl *a* and transfer excitation energy from chlorosomes to the RCs.

All species are strictly anaerobic phototrops with only carbon source in a form of CO_2. Sulfide is used as an electron donor and sulfur source. Elemental sulfur is formed and accumulated in a form of sulfur globules outside the cells.

3.2 Green Nonsulfur Bacteria

Members of this group (also called Chloroflexi) are physiologically more diversed than Chlorobi. This can be simply demonstrated by the fact that many of them are capable of both chemotrophic and phototrophic growth under aerobic or anaerobic conditions respectively (HANADA – PIERSON, 2006). Some of the Chloroflexi are not even photosynthetic and grow chemoheterotrophically under aerobic conditions. Only some representatives of a subgroup Chloroflexaceae contain chlorosomes and they are often referred to as green filamentous bacteria. They contain type II reaction center and apart from chlorosomes, they have in cytoplasm embedded light harvesting complex (LHC) functionally similar to LH1 complex of purple bacteria assigned B808 – 866 (XIN et al., 2005). Lots of Chloroflexaceae are able to respire in dark under aerobic conditions at the cost of suppressed photosynthetic apparatus.

3.3 Purple Sulfur Bacteria

Purple bacteria in general have been isolated from extreme environmental areas including hot, cold, acidic, alkaline, and hypersaline environments. The major photosynthetic pigments are BChl *a*,*b* and a broad range of carotenoids such as spirilloxanthin, rhodopinal spheroidene, and okenone (TAKAICHI, 2004). Purple sulfur bacteria are specific for intracellular storage of oxidized sulfide in a form of elemental sulfur S_0. Phototrophic growth prevails for most of the species. Sulfide, thiosulfate, or hydrogen is used as an electron donor. Apart from that, small amount of organic carbon source can be assimilated by some species, as

well as possible dark growth, which predominantly serves to overcome temporary oxygenic conditions (KAMPF – PFENNING, 1980).

3.4 Purple Nonsulfur Bacteria

Purple non-sulfur bacteria is an extremely diversed group. Despite the fact that they are called non-sulfur, they can withstand and grow up to 0.5 mM sulfide concentrations. Distinction between sulfur and non-sulfur bacteria is based on the difference in sulfur storage as purple non-sulfur bacteria do not store it. They transfer it outside the cell in a form of globules (MADIGAN – JUNG, 2008). Some species are sensitive to oxygen, but majority is able to grow under aerobic conditions in dark, which causes suppression of synthesis of photosynthetic pigments and cultures become almost colorless.

3.5 Heliobacteria

Representatives of this group are strictly anaerobic anoxygenic photoheterotrophs containing BChl *g* as the main photosynthetic pigment (GEST – FAVINGER, 1983; BROCKMANN – LIPINSKI, 1983) and lacking BChl *a*. That results in unique spectroscopic properties as the main absorption peak originating from BChl *g* is near 785 nm. BChl *g* is sensitive to oxygen and in a case of air exposure, it is oxidized to BChl *a* and the 785 nm peak is blue-shifted to around 746 nm (ASAO – MADIGAN, 2010). Another unique property is that heliobacteria lack peripheral antennas and all photocomplexes are restricted only to cytoplasmic membrane (MILLER et al., 1986).

Heliobateria are from the phylogenetic point of view mostly related to cyanobacteria (oxygenic-photosynthetic prokaryotes, also called blue-green algae) and that has led to assumption that they should be able to produce endospores. It was found that this property is universal among heliobacteria (KIMBLE-LONG – MADIGAN, 2001). Their most common habitat is soil or hot springs but some aquatic species were found as well.

3.6 Chlorosomes

Reaction centers of photosynthetic organisms are in general of two types. Green bacteria and heliobacteria have photosystem I-like RC, also called FeS-type RC. On the other hand, purple bacteria and green non-sulfur bacteria have photosystem II-like RC, also called quinone-type RC. Higher plants combine both types of reaction centers and photosystems to take advantage of their interconnection. Although there are only two types of reaction centers, organisms living in different environments regarding light intensity and solar spectrum density have to adapt to their environments. That is done by differentiation of their light-harvesting antennas. One such antenna system has developed for light-harvesting in anaerobic and extremely low-light conditions. These structures are nowadays called chlorosomes (originally denoted as "Chlorobium vesicles" (GEST et al., 1963)) which exhibit some unique features such as prevailing pigment-pigment interac-

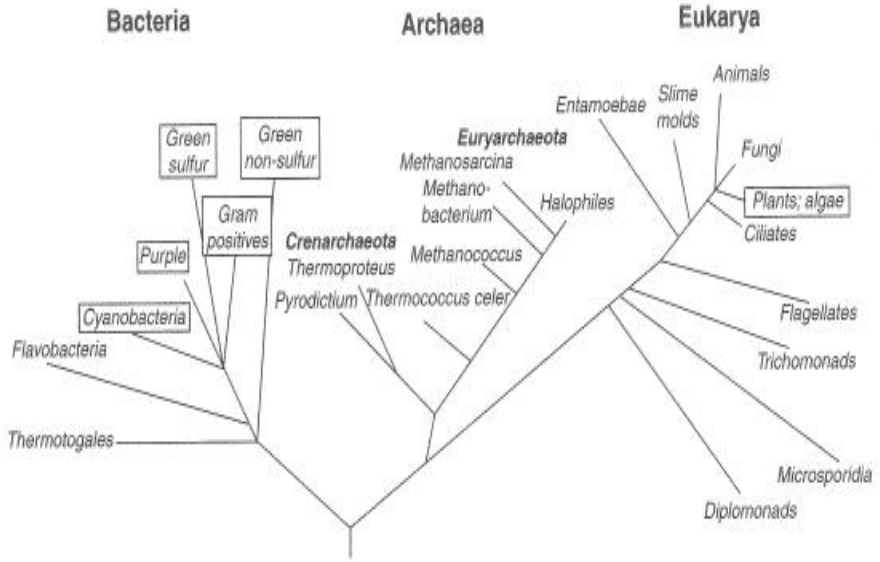

Figure 3.1: Phylogenetic tree based on subunit rRNA sequences analysis. Groups containing photosynthetic organisms are boxed (BLANKENSHIP, 2002).

tion (instead of pigment-protein), self-assembly, and big size. Because of that, chlorosomes have become a promising inspiration for artificial photosynthesis.

Chlorosomes are main light-harvesting complexes occurring in organisms within two bacterial phyla, Chlorobi and Chloroflexi (see section 3.1, 3.2). These organisms occur mainly in stratified lakes and microbial mats in depth up to 100 m, where light intensity is lowered by a factor 10^{-6} of the surface magnitude (FRIGAARD – BRYANT, 2006). One of the most remarkable species is a green sulfur bacterium discovered near black smoker in depth 2391 m below sea-level, which acquire excitation energy for conducting photosynthesis from geothermal energy from the hot smoker (BEATTY et al., 2005). The insufficient photon flux in extremely low-light conditions is compensated by high BChl content which can correspond up to 30 % of the carbon content of the whole cell (BORREGO et al., 1999). This high pigment content is enabled by prevailing pigment-pigment interactions and self-assembly of chlorosomes which do not require excessive energy-consuming protein synthesis. The protein to BChl *c* ratios found for chlorosomes differ depending on the strain and purity of the preparation, but ranges from approximately 2.2:1 (w/w) in *Chloroflexus aurantiacus* (*Cf. aurantiacus*) (FEICK – FULLER, 1984) to 0.5:1 (w/w) in *Chlorobaculum tepidum* (*Cba. tepidum*) (CHUNG et al., 1994). These ratios are much lower than in other pigment-protein complexes, for example protein to pigment ratio for FMO complex is 6.3:1 (BLANKESHIP et al., 1995).

3.6.1 Pigments

As regards pigment content, only Bchl *c*, *d*, *e* are found in aggregated form in chlorosomes. Cultures containing BChl *c* or *d* aggregates appear dark green whereas chlorosomes containing BChl *e* appear brown due to strong absorption band of BChl e in the region of 500 – 550 nm (FRIGAARD et al., 2000). It was

calculated from the chemical measurements that chlorosome from *Cba. tepidum* contains approximately 200 000 BChl *c* molecules, 2500 BChl *a* molecules (found in FMO complex and CsmA protein (MONTANO et al., 2003; BRYANT et al., 2002)), 20 000 carotenoid molecules, 15 000 chlorobiumquinone molecules and 3000 menaquinone-7 molecules. The BChls from green sulfur bacteria chlorosomes are methylated in the C-8^2 and C-12^1 positions which results in a red-shifted BChl absorption maximum and broadening of the spectrum. This homologation process increases hydrophobic interaction between the BChls facilitating formation of larger chlorosomes that results in better adaptation for growth at low-light conditions (HUSTER – SMITH, 1990).

Carotenoids absorb light in the region of 400 – 550 nm and subsequently transfer the excitation energy to chlorosome BChls or BChl *a* (present in the baseplate) via singlet state. Fluorescence measurements indicated efficiency of excitation energy transfer from carotenoids to BChl *c* to be 50 – 80 % in isolated chlorosomes (MELØ et al., 2000). Another role of carotenoids is structural as they maintain the organization of chlorosomal baseplate (ARELLANO et al., 2001). Carotenoids together with quinones have as well the ability to quench BChl triplet states (FRIGAARD et al., 1997; MELØ et al., 2000; CARBONERA et al., 2002). That is very important while the long-lived excited triplet state of BChl can give rise to reactive oxygen species via reaction with the triplet ground state of oxygen which is not spin-forbidden as the relaxation of BChl from excited triplet state to the ground state.

Small amount of BChl *a* is present in chlorosome, the ratio of BChl *a* to BChl *c* is 0.01 for *Cba. tepidum* chlorosome. It is bound to CsmA protein and play important role in excitation energy transfer from chlorosome BChl antenna to the reaction center (BLANKESHIP et al., 1995).

3.6.2 Structure of Chlorosome

Although chlorosomes are similar among Chlorobi and Chloroflexi phyla (opposed to the reaction centers and peripheral antennae which support concept of lateral transfer of chlorosomes between the two phyla (STACKEBRANDT et al., 1996)), they are different in many ways as well. Main difference is lacking FMO protein in the case of green filamentous bacteria where chlorosome interacts directly with LH1-type antenna complex B808 – 866 ("B" stands for "bulk" and the number denotes the main absorption wavelength of the complex), which is an intermediate between chlorosome and RC in excitation energy transfer (XIN et al., 2005). Schematic structure of chlorosome is depicted in figure 3.2. Both types of chlorosomes contain a baseplate structure which is constituted from CsmA protein and acts as an attachment site of the chlorosome either to the FMO protein or the B808 – 866 complex (FRIGAARD – BRYANT, 2006). BChl aggregates are encapsulated in monolayer of protein-lipid envelope with high content of glycolipids (SØRENSEN et al., 2008). Overall size of chlorosome is typically 100 – 200 nm in length and 30 – 100 nm in width for green sulfur bacteria and slightly smaller for green filamentous bacteria (FRIGAARD et al., 2005). The great variability of chlorosome size (as well as pigment composition) is due to different growth conditions (OELZE – GOLECKI, 1995).

Aggregation of BChls shifts the absorption maximum of Q_y band to the red by

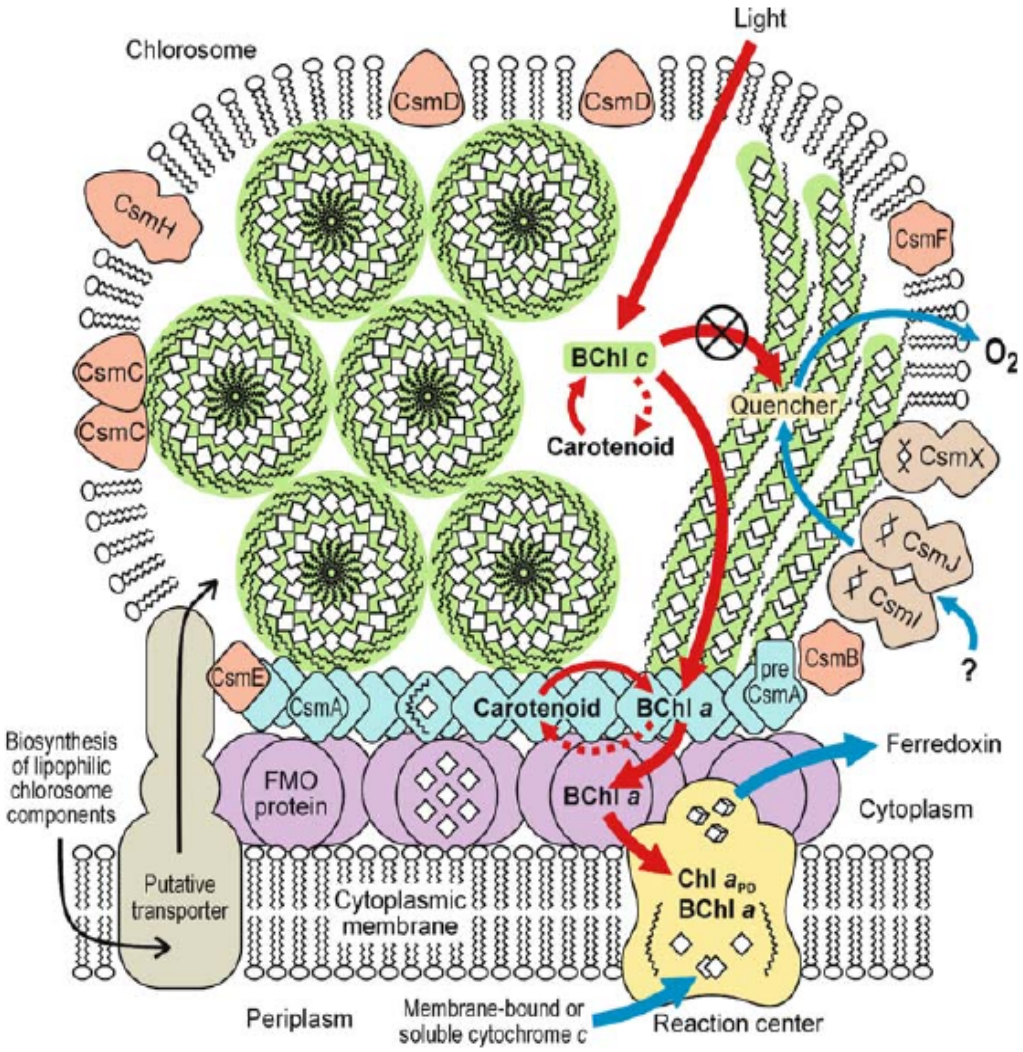

Figure 3.2: Model of the chlorosome and photosynthetic membrane in *Cba. tepidum*. Singlet excitation energy transfer is shown by solid red, quenching of excited BChl triplets by carotenoids is shown by dotted red lines and electron transfer is shown by blue lines. Modified from (FRIGAARD et al., 2005) by (FRIGAARD – BRYANT, 2006).

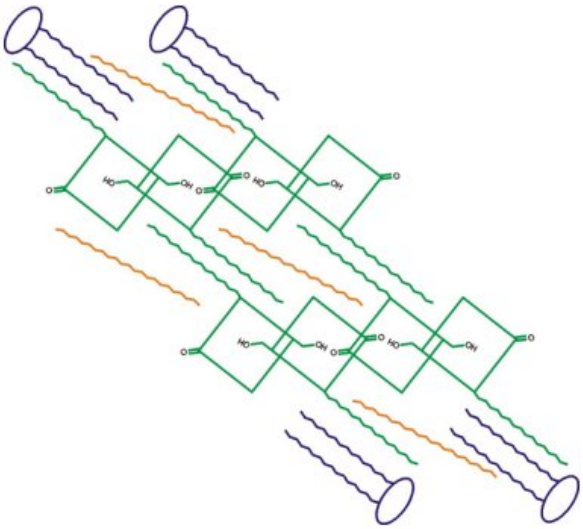

Figure 3.3: Scheme of lamellar organization and interactions between bacteriochlorophylls (green), carotenoids and quinones (orange), and lipids (violet) (KLINGER et al., 2004).

70 – 80 nm (peaks between 745 and 760 nm for BChl c containing species) in comparison with monomeric forms in organic solvents (BLANKESHIP et al., 1995). The red shift is caused by strong excitonic coupling between BChl molecules. Detailed structure of BChl aggregates on a molecular level is not known yet, but several models have been proposed. The two most prevailing in literature are "parallel" (HOLZWARTH – SCHAFFNER, 1994) and "antiparallel" model (NOZAWA et al., 1994). On the long range scale several rod-like elemental models of BChl aggregates have been presented (NOZAWA et al., 1994; MATSUURA et al., 1993). These models are challenged by lamellar model of aggregates where the fundamental structural unit is antiparallel dimer (PŠENČÍK et al., 2004). Based on cryo-electron microscopy and nuclear magnetic resonance of *Cba. tepidum* mutant containing only BChl *d*, syn-anti stacking model forming concentring nanotubes with BChls arranged in helical spirals was recently proposed (GANAPATHY et al., 2009).

According to the lamellar model esterifying alcohol chains point to both sides of lamella and hydrophobic interaction between esterifying alcohols from adjacent lamellas stabilizes the aggregate. Other lipophilic components such as carotenoids and quinones occupy the intra-lamellar space (figure 3.3). The amount of carotenoids and quinones contained between lamellas as well as lamellar spacing (ranging from 10 Å to 35 Å) is proportional to the length of the esterifying alcohol (PŠENČÍK et al., 2010).

3.6.3 Bacteriochlorophyll Aggregates *In Vitro*

Chlorosomal bacteriochlorophylls exhibit spontaneous aggregation *in vitro*. Pioneer in studying BChl aggregation was A. A. Krasnovsky who first proposed the pigment organization model for chlorosomes in form of BChl aggregated oligomers (KRASNOVSKY – BYSTROVA, 1980). Aggregation occur in both nonpolar solvents and aqueous solutions with similar optical properties (such as absorption,

fluorescence, circular and linear dichroism spectra) to native chlorosomes. Non polar solvent induced aggregation was demonstrated using zinc(II) methyl bacteriochlorophides in hexane-methylen chloride (200:1) solution (SMITH – KEHRES, 1983), as well as in case of extracted BChl *c* from *Cf. aurantiacus* in hexane (BRUNE et al., 1987b,a). These studies showed important role of central atom and hydroxyl group at 3^1 position in BChl. Other studies pointed to oligomers acquired in water-saturated CCl_4 (OLSON – J.P.PEDERSEN, 1990; UEHARA – OLSON, 1992). Aggregation of BChl *c* in aqueous systems was observed in presence of detergents or lipids (MILLER et al., 1993; HIROTA et al., 1992). Spectral properties were similar to native chlorosomes and aggregates exhibited same reversible shift after 1-hexanol treatment as in chlorosomes (BLANKESHIP et al., 1995). In general, hydrophobic interaction plays a key role in inducing BChl aggregation and therefore non-polar molecules such as quinones and carotenoids can induce the aggregation as well as non-polar solvents (ALSTER et al., 2008). Research expanding these studies into area of synthetic and semisynthetic tetrapyrroles emerged recently as reviewed in (BALABAN, 2005).

3.6.4 Excitation Quenching

Green sulfur bacteria are strictly anaerobic organisms (see section 3.1) containing low potential Fe-S type RC similar to photosystem I but do not posses any active mechanism providing removal of oxygen from their environment. However ability to sustain terminate exposure to oxygen without damage by reactive oxygen species would be advantageous as green sulfur bacteria are found in many different environments, which happen to be occasionally exposed to oxygen (BLANKESHIP et al., 1995).

The solution green bacteria utilize is redox dependent excitation quenching. This phenomenon has been observed in whole cells, isolated membranes, and purified chlorosomes and it is therefore attributed to antenna systems (WANG et al., 1990). The energy transfer efficiency is reduced from almost 100 % to 10 % together with excited state life-time decrease from 50 – 100 ps to 10 – 15 ps. The midpoint potential in chlorosomes was determined to -146 mV versus normal hydrogen electrode at pH 7 with a pH dependence of -59 mV per pH unit in the pH range 7 – 10 (BLANKENSHIP et al., 1993). The quenching mechanism is not sufficiently understood, but it has been proposed to involve BChl *c* radicals based on the excited state life-times measured in both chlorosomes and BChl *c* oligomers (vanNoort et al., 1997). However, quinones play major role in redox-dependent quenching in both chlorosomes and BChl *c* aggregates (FRIGAARD et al., 1997, 1998; ALSTER et al., 2008). Chlorobiumquinone seems to be the most effective quencher. Slow reduction of the quencher occurs (in the case of chlorobiumquinone to the semiquinone) after restoring anaerobic conditions. CsmI, CsmJ seem to be involved in the reduction of a quencher, and possibly CsmX proteins as well (LI et al., 2006).

This mechanism is almost completely missing in *Cf. aurantiacus* since it does not produce such a strong reductans in the reaction center and it can easily adapt to aerobic conditions (FRIGAARD – BRYANT, 2006).

4. Hole Burning

Hole burning spectroscopy (HB) is in general saturation spectroscopy technique which reveals features of the homogeneous line shape hidden in the inhomogeneously broadened spectrum. The phenomenon of burning spectral hole was firstly demonstrated in NMR spectroscopy in 1948. Since then, many methods and applications have been introduced in almost all spectroscopy fields, from NMR, dielectric spectroscopy to IR and optical spectroscopy (TRANTER et al., 2000). First application of spectral hole burning (SHB) to chromophores in crystalline matrices at low temperature has occurred in 1974 (GOROKHOVSKII et al., 1974; KHARLAMOV et al., 1974).

SHB applied for photosynthetic systems can be used for investigation of exciton level structure, energy and electron transfer, role of phonons and heterogeneity of the frequencies of active optical transitions and their strengths (Franc-Condon factors). The basic principle of SHB is excitation of spectrally narrow set of chromophores from inhomogeneous spectrum using narrow band laser as the transition to the ground state is either blocked (persistent hole burning) or delayed (transient hole burning). Reason for blocking or delaying the relaxation can be either photochemical reaction of excited molecules denoted as photochemical hole burning (PHB) or rearrangement of the host matrix (denoted nonphotochemical or photophysical hole burning NPHB) (RAJA et al., 1996). Molecules which underwent such a process absorb light at different wavelengths and form photoproduct (also called antihole, see figure 4.1).

4.1 Molecular Absorption Spectra in Glassy Matrix

Let us assume the two-level system of the impurity center in glassy matrix. This assumption is relevant as the majority of photoactive molecules undergo radiative transitions only between S_1 a S_0 states. After the excitation of the dopant to the higher electronic state, the molecule undergoes fast nonradiative relaxation to the S_1 state.

Pure electronic molecular transition appears in the absorption spectrum as a narrow zero phonon line (ZPL) which is characterized by the amplitude and the ZPL line width (see figure 4.2). According to the quantum theory of electromagnetic field, the ZPL line width determines the excited state lifetime (DAVYDOV, 1978). Transition probability depends also on the density and frequency of the host matrix vibronic states. These vibrations give rise to a broad phonon wing which is strongly dependent on the temperature (MOERNER, 1988). Because of that, it is crucial to maintain sufficiently low temperature for observing ZPL lines.

4.2 Spectral Hole Shape Theory in HB

General line shape of single molecule can be described as the sum of zero phonon part $z(\omega)$ with homogeneous line width $\Delta\omega_h$ and phonon wing $p(\omega)$. Normalized

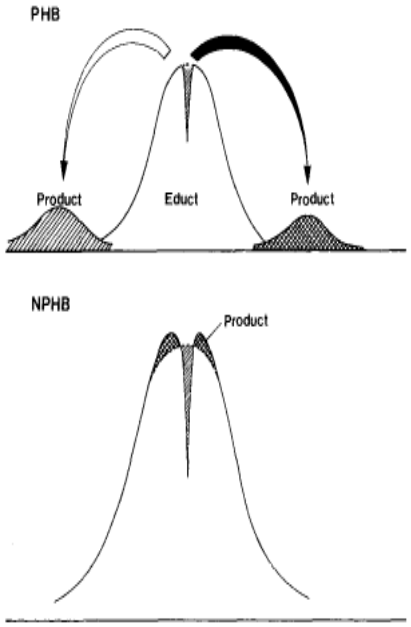

Figure 4.1: Comparison of spectral distribution of photoproduct after PHB and NPHB (FRIDRICH – HAARER, 1984).

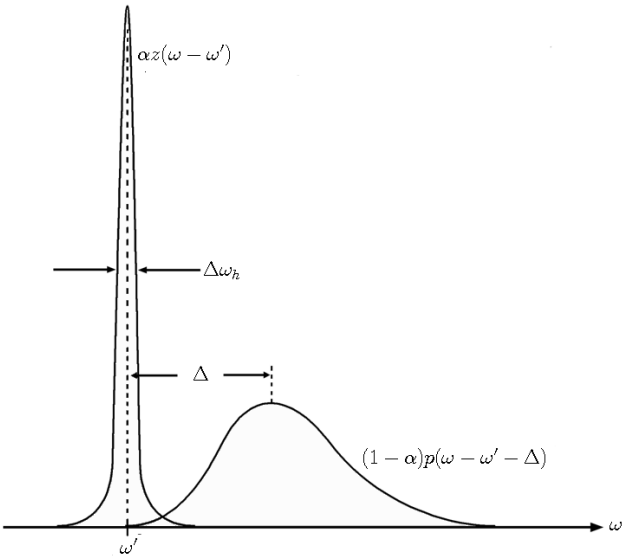

Figure 4.2: Molecular spectral line shape in crystaline matrix.

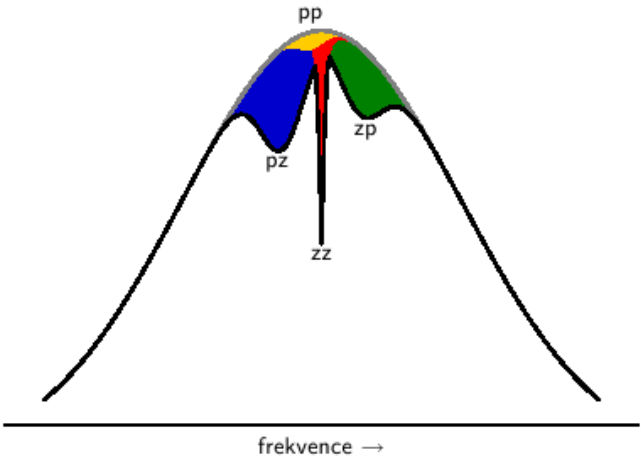

Figure 4.3: Schematic view of four terms contributing to the hole shape (DĚDIC, 2000).

line shape $g(\omega)$ can be then written as

$$g(\omega - \omega') = \alpha z(\omega - \omega') + (1 - \alpha)\, p(\omega - \omega' - \Delta) \tag{4.1}$$

where $g(\omega - \omega')$, $z(\omega - \omega')$ and $p(\omega - \omega')$ are normalized functions, α is so-called Debye-Waller factor, which characterize amount of electron-phonon interaction between dopant and matrix and Δ is shift of the phonon wing in respect to ZPL (MOERNER, 1988), which corresponds to the half of the Stokes shift. The molecule absorbs light through the ZPL as well as through the phonon wing during the laser irradiation with frequency ω_{L}. Number of molecules which undergo interaction with laser light during the irradiation is (FRIDRICH – HAARER, 1984)

$$\rho_\tau(\omega') = \rho_0(\omega') \exp[-W(\omega_{\mathrm{L}}, \omega')\Phi\tau] \tag{4.2}$$

where $\rho_0(\omega')$ is number of molecules before irradiation, Φ is quantum yield of interaction, $W(\omega_{\mathrm{L}}, \omega')$ is transition probability per unit of time and τ is burning time. Convolution of ρ_τ with spectral line shape (4.1) gives the final absorption spectrum $A_\tau(\omega)$:

$$A_\tau(\omega) = \sigma \int_{-\infty}^{+\infty} \rho_\tau(\omega')\, [\alpha z(\omega - \omega') + (1 - \alpha)\, p(\omega - \omega' - \Delta)]\, \mathrm{d}\omega' \tag{4.3}$$

Subtracting of the $A_\tau(\omega)$ from the initial spectrum $A_0(\omega)$ together with assumption that ZPL line $z(\omega - \omega')$ is narrow with respect to ρ and p makes it possible to overwrite the expression $A_0(\omega) - A\tau(\omega)$ as a sum of four terms (see figure 4.3)

$$zz(\omega) = \sigma\, \alpha\, \rho_0(\omega_{\mathrm{L}}) \left\{ 1 - \int_{-\infty}^{+\infty} \exp\left[-\frac{\alpha\sigma I \Phi\tau}{\hbar\omega_{\mathrm{L}}}\, z(\omega_{\mathrm{L}} - \omega') \right] z(\omega - \omega')\, \mathrm{d}\omega' \right\} \tag{4.4}$$

$$zp(\omega) = \sigma\rho_0(\omega_\mathrm{L})(1-\alpha)p(\omega-\omega_\mathrm{L}-\Delta)\left\{1-\exp\left[\frac{-\alpha\sigma I\Phi\tau}{\hbar\omega_\mathrm{L}\delta_\mathrm{h}}\right]\right\}\delta_\mathrm{h} \tag{4.5}$$

$$pz(\omega) = \sigma\alpha\rho_0(\omega_\mathrm{L})\left\{1-\exp\left[-\sigma(1-\alpha)\frac{I\Phi\tau}{\hbar\omega_\mathrm{L}}p(\omega_\mathrm{L}-\omega-\Delta)\right]\right\} \tag{4.6}$$

$$pp(\omega) = \sigma(1-\alpha)\int_{-\infty}^{+\infty}\left\{1-\exp\left[-\frac{\sigma I\Phi\tau}{\hbar\omega_\mathrm{L}}(1-\alpha)p(\omega_\mathrm{L}-\omega'-\Delta)\right]\right\}p(\omega-\omega'-\Delta)\mathrm{d}\omega' \tag{4.7}$$

where the term $zz(\omega)$ is attributed to the narrow zero phonon hole which shape depends apart from homogeneous line width also on experimental parameters, such as laser intensity I and burning time τ (FRIDRICH – HAARER, 1984). The exponential term in equation (4.4) can be expanded into the Taylor series with neglected second and higher order terms for the sufficiently short burning times. Herewith we obtain

$$zz(\omega) = \frac{I\tau}{\hbar\omega_\mathrm{L}}\sigma^2\alpha^2\Phi\rho_0(\omega_\mathrm{L})\int_{-\infty}^{+\infty}z(\omega_\mathrm{L}-\omega')z(\omega-\omega')\mathrm{d}\omega' \tag{4.8}$$

which is a form of convolution integral. It can be solved analytically if we assume that the spectral line $z(\omega)$ has Lorentzian profile with full width at half maximum FWHM$=\delta_\mathrm{h}$

$$z(\omega) = \frac{\delta_\mathrm{h}}{2\pi}\frac{1}{(\omega-\omega_\mathrm{L})^2+\delta_\mathrm{h}^2} \tag{4.9}$$

By solving the integral in (4.8) we get to the final term for ZPL line $zz(\omega)$

$$zz(\omega) = \frac{I\tau}{\hbar\omega_\mathrm{L}}\sigma^2\alpha^2\Phi\rho_0(\omega_\mathrm{L})\frac{\delta_\mathrm{h}}{\pi}\frac{1}{(\omega-\omega_\mathrm{L})^2+\delta_\mathrm{h}^2} \tag{4.10}$$

which again corresponds to the line with Lorentzian profile, but this time with FWHM $= 2\delta_\mathrm{h}$. Assumption of the finite width of burning laser spectral line δ_L gives for the hole width in case of zero burning dose term

$$\delta_\mathrm{ZPL} = 2\delta_\mathrm{h} + \delta_\mathrm{L} \tag{4.11}$$

4.3 Implication for Time Constants

General formula expressing the relationship between the spectral hole width $zz(\omega)$ and time constants of the processes studied in the HB experiment provides in case of neglecting inhomogeneous broadening such as Doppler broadening in units of 2π/s (FRIDRICH – HAARER, 1984)

$$\delta_\mathrm{h} = \frac{1}{T_2}\sqrt{1+\omega_1^2T_1T_2} \tag{4.12}$$

where ω_1 is a Rabi frequency which is proportional to the amplitude of the electric field vector, T_1 is the excited state lifetime in the matrix and T_2 is optical

dephasing time. If the following condition is fulfilled (when burning intensity is small)

$$\omega_1^2 \ll \frac{1}{T_1 T_2} \tag{4.13}$$

we can neglect the second term under the root in equation (4.12) and therefore simplified to

$$\delta_{\mathrm{h}} = \frac{1}{T_2} = \frac{1}{T_1} + \frac{2}{T_2^*} \tag{4.14}$$

where T_2^* is the pure dephasing time which is strongly dependent on temperature. Pure dephasing time can be neglected in the case that hole widths are independent on temperature (see section 7.2). Under previous assumption together with relation $\mathrm{FWHM} = 2\delta_{\mathrm{h}}$ and after conversion to seconds, we get the relationship between the homogeneous hole width and the excited state lifetime:

$$\delta_{\mathrm{h}} = \frac{1}{\pi \mathrm{c} \mathrm{T}_1} \tag{4.15}$$

where c is the speed of light. That means that relation between hole width and excited state lifetime is inversely proportional and hence advantageous for investigation of rapid processes in photosynthesis, including the excitation quenching in BChl *c* aggregates.

So-called fluence broadening of the hole occurs during the burning process. After the hole is primarily burnt, saturation takes place and the burning process continue only at the edges which broadens the hole. For the high burning doses can be the exponential term from (4.4) excluded from the integral because it changes a little with respect to $z(\omega)$. The ZPL hole width then increases as a square root of $I\tau$. This relationship describes nondispersive burning kinetics. Various distribution of states with different energy barriers between states in two-level system causes perturbations from nondispersive kinetic. In the case of hyperbolic distribution of the states, the kinetic is on the contrary dispersive and the hole widths increase as $(I\tau)^{\frac{1}{4}}$. That is why the fluence dependence obtained from HB experiment is fitted using a function in form

$$\delta_{\mathrm{ZPL}} = \delta_{\mathrm{h}} + a(I\tau)^b \tag{4.16}$$

where the value of the parameter b determines whether the kinetic is dispersive or nondispersive (FRIDRICH – HAARER, 1984).

5. Experimental Setup

Hole burning is sophisticated experimental technique whose realization involves broad spectrum of physics fields, such as laser and low-temperature spectroscopy. That includes optics, cryo-technique and other complex control systems for ensuring stable experimental conditions throughout the experiment. The original experimental set-up is schematically depicted in figure 5.2.

5.1 Laser Technique and Optics

Laser technique in hole burning experiment consist of tunable Littman/Metcalf external cavity diode laser, model TEC 500 from Sacher Lasertechnik utilizing master-slave tapered amplifier configuration. Master laser is controlled by Pilot-PZ 500 controller and tapered amplifier (slave laser) is controlled via PilotPC 3000 controller. Schematic drawing of the Littman/Metcalf amplified system is shown in figure 5.1. The laser light is generated by radiative transitions in a p-n junction induced by current flow. When the current grows over threshold value, stimulated emission exceeds spontaneous emission and non-radiative relaxation. Amplification of the signal is realised by tapered amplifier. Tunability of the laser emission wavelength is based on rotation of the diffraction grating through both turning a screw (wide range tuning) and piezoelectric transducer (medium range tinning). The most sensitive tinning can be achieved by changes in current flow through the laser diode. Whole laser system parameters are summarized in table 5.1. Laser beam is led through the system of prisms to the sample space in a cryostat with the incident beam area of $\sim 0.6 - 0.8\,\mathrm{mm}^2$.

5.2 Cryogenic Technique

Basic element of the cryogenic technique was a cryostat SVT - 300 manufactured by Janis Research with a capacity of 5 litres of liquid helium (LHe). The cryostat is made of stainless steal and consist of liquid helium and liquid nitrogen reservoirs which are surrounded by an evacuated space to minimize heat conductivity. The liquid nitrogen reduces radiation losses between liquid helium and

Parameter	Value
Power	1320 mW at 780 nm
Tunability	764,5 – 799,7 nm
Current tuning	$\sim$ 0.17 GHz/mA
Temperature tuning	$\sim$ 24 GHz/°C
Piezo-tuning	$\sim$ 1 GHz/V
Single mode tuning	40 GHz at 780 nm
Line width (50 ms)	$<$ 1 MHz
Line width (20 s)	$<$ 5 MHz

Table 5.1: Laser system parameters.

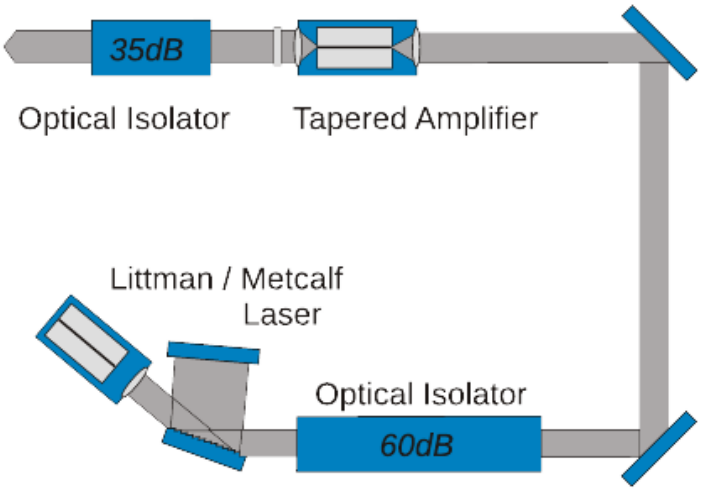

Figure 5.1: Illustrative scheme of a laser system in Littman/Metcalf amplified configuration used for hole burning experiment.

room temperature (the power emitted per unit area of the surface of a black body is directly proportional to a fourth power of its absolute temperature). A tail extension enables optical access to a sample through O-ring sealed windows. Sample is attached to a probe and inserted into a sample tube. Helium flow into the sample space is regulated by a helium valve that enables partial temperature control. This configuration is called flow cryostat with detachable tail Dewar. Two temperature sensors are installed in a sample tube, one is at a heating spiral and another is installed at the sample mount for a precise control of the sample temperature. Heating spiral is the second possible way to control temperature if connected to automatic temperature controller. Third possible way is variation of pumping rate of the helium vapours, which also gives opportunity to achieve temperatures as low as 1.7 K if the helium valve is closed. Temperature of ~ 1.9 K is achievable with open helium valve in flow cryostat mode (see section 5.5).

Two stage rotary vane pump and diffusion pump are used for evacuation of the Dewar. Rotary vane pump works on the principle of the cyclic rotation of the excentric cylindrical rotor in the cast metal stator. There are plates fixed to the rotor which are pressed to the stator wall by a spring in order to divide the cavity in two separate spaces. The gas is suctioned into the larger space which consequently gets smaller upon rotation of the stator. The gas is compressed and after exceeding atmospheric pressure is the gas released out from the pump by pressure-relief valve. When the vacuum is in the order of ~ 1 Pa, it is possible to start evacuating using diffusion pump. The pumped gas diffuses into a stream of oil vapours heated by a heating spiral. Vapours are then cooled by a water circuit and they sink towards outlet in the primary vacuum where the vapours condensate and the pumped gas is released. Possible back-flow of the vapours to the cryostat is avoided by cold trap filled with liquid nitrogen. This procedure leads to vacuum order of $\sim 10^{-3}$ Pa. After the cryostat is filled with liquid helium the pressure decreases by another order of magnitude because of condensation of

the remaining gas on the wall of the helium Dewar.

5.3 Absorption Measurements

Absorbance is a measure of light absorbed by a sample. In spectroscopy is absorbance A_λ at wavelength λ defined as

$$A_\lambda = -\log_{10}\left(\frac{I}{I_0}\right) = -\log_{10} T \tag{5.1}$$

where I and I_0 are intensities of transmitted and incident light respectively, and T is transmittance. Following the Lambert–Beer law, absorbance is linearly proportional to the concentrations of the absorbers in the sample

$$A_\lambda = \epsilon_\lambda l c \tag{5.2}$$

where ϵ_λ is extinction coefficient at given wavelength, l is sample path length and c is a molar concentration of the absorber in the sample. Absorbance measurement is realised in two-channel configuration in our experiment which limits instability of lamp (see section 5.5). We measure transmittance under an assumption that the sample is low scattering.

Wolfram lamp Oriel with 250 W radiometric source is used for absorbance measurement and its intensity is controlled via feedback from Oriel-Light intensity controller. The intensity controller however measures the intensity over the whole spectrum of the lamp, which does not provide sufficient information about the light intensity at the particular wavelength during the absorption measurement. That leads to the requirement for two-channel configuration (see section 5.5). The light from the lamp passes through double-grating monochromator Jobin Yvon HRD 1, with slits width of 0.15 mm. That results in resolution of $\sim 1.4\,\mathrm{cm}^{-1}$ at 780 nm. Monochromatic light then passes through a chopper and optical system (see 5.3) where it is divided into signal and reference channels. Reference channel strikes directly a photocathode of a photomultiplier and signal channel is focused into the sample in the cryostat. Light transmitted through the sample enters another photomultiplier. Both photomultipliers are Hamamatsu R943-02 cooled by photomultiplier cooler C10372 from Hamamatsu with water circuit. They are connected to the same power supply in order to decrease the difference of the voltage on both photomultipliers, which was set to 1600 V. Signals from the photomultipliers are amplified via lock-in amplifiers SR 830 DSP by the synchronous detection. It works on the principle of amplification of the signal modulated by the chopper with only the same frequency and phase. Each data point consists of an average of 50 accumulations and is subsequently saved on the PC. Whole measurement is processed by a driver written in LabVIEW 8.5.

5.4 Hole Burning Spectra

Hole burning spectra are obtained with the 0,02 nm step within the range of ±1 nm around the burning frequency. Spectra before the burning are also measured as the hole spectra are obtained as the difference absorption spectra (DAS).

The formula for DAS can be derived with the application of eq. (5.1):

$$\Delta A(\lambda) = A_{aft}(\lambda) - A_{bef}(\lambda) = -\log_{10}\left(\frac{I^{sig}_{aft}(\lambda)\cdot I^{ref}_{bef}(\lambda)}{I^{sig}_{bef}(\lambda)\cdot I^{ref}_{aft}(\lambda)}\right) \tag{5.3}$$

where indices *bef* and *aft* mean values before and after laser irradiation and indices *sig* and *ref* mean values from signal and reference channel respectively. After the initial spectra before burning were obtained, the burning with the diode laser and spectra accumulation take turns with increasing burning period in order to get a fluence dependence. That means the dependence of the hole width on the burning dose $P{\cdot}t/A$, where P is the laser power, t is burning time and A is the laser beam area. The fluence dependence is extrapolated to the zero burning dose according to eq. (4.16) to get the natural hole width and the excited state lifetime.

5.5 Setup Improvement

Experimental results and experiences obtained in previous years (PALEČEK, 2009) naturally led to many suggestions for experimental set-up improvements in order to make possible hole burning at longer wavelengths, to suppress lamp instability, to achieve higher signal to noise ratio (S/N ratio) and to get rid of bubbles from boiling helium scattering the measuring light. Original experimental set-up is depicted in the figure 5.2.

5.5.1 Diode Laser

Past experiments conducted with dye laser Spectra-Physics model 375B which was pumped by an argon laser Coherent Sabre Innova, we encountered problems with dye laser radiation stability and with tuning the longer laser line wavelengths by birefringent filter since we were using wavelengths on the edge of dye emission as well as on the edge of laser mirrors spectral reflexivity. That limited hole burning experiment only for wavelengths up to 777.1 nm and for laser powers up to 100 mW. Recently bought diode laser TEC 500 with tapered amplifier from Sacher Lasertechnik (see section 5.1) was acquired with expectations not only to enable burning at longer wavelengths with higher laser power but moreover to provide fast and accurate way to measure the hole burning spectra without need of the lamp, monochromator etc.. That should have been made possible thanks to an accurate and single mode tuning and extremely narrow laser line (see table 5.1). However, the reality after the delivery and testing was slightly different.

The main disadvantage found was spontaneous shift of laser frequency in time when neither direction is preferred and rate of the shift was $\sim$1 GHz/min. Our assumption is that the frequency shifts occur as a consequence of varying temperature of the master laser diode. Measurement of the laser line with sufficient resolution was realized using scanning Fabry-Perot etalon Sigma Physics, model 470 interferometer (see figure 5.4). Laser line spectral position was measured with optical spectral analyzer ADCMT 8342. It utilizes Fourier spectrum system with a Michelson interferometer with spectral resolution of 0.01 nm. Moving of the laser line precluded from the possibility of collection absorption spectra utilizing

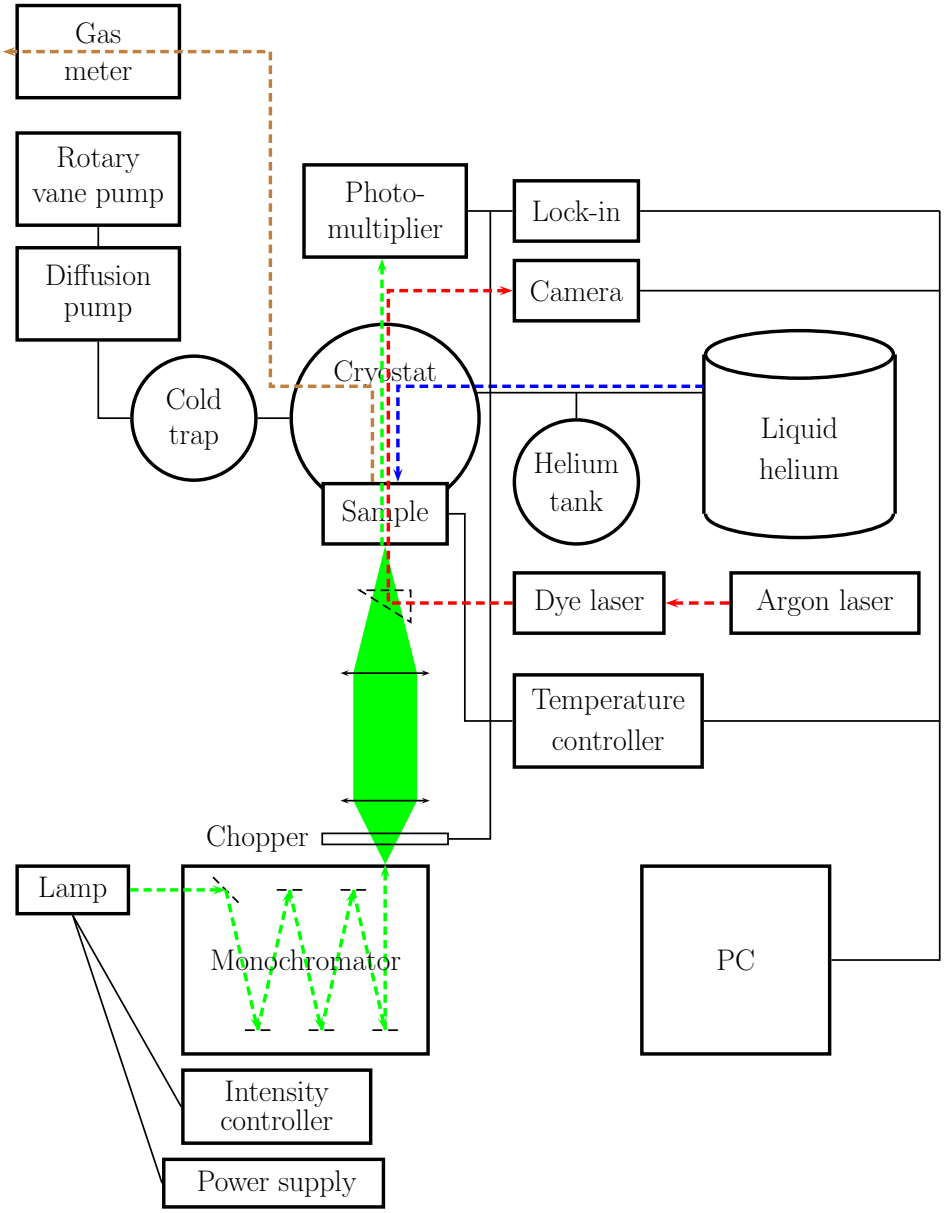

Figure 5.2: Illustrative scheme of the original experimental set-up for spectral hole burning experiment in the absorption spectrum at LHe temperature. Green color indicates light from the wolfram lamp, red is the laser radiation, blue color depicts LHe and helium vapours are indicated by brown.

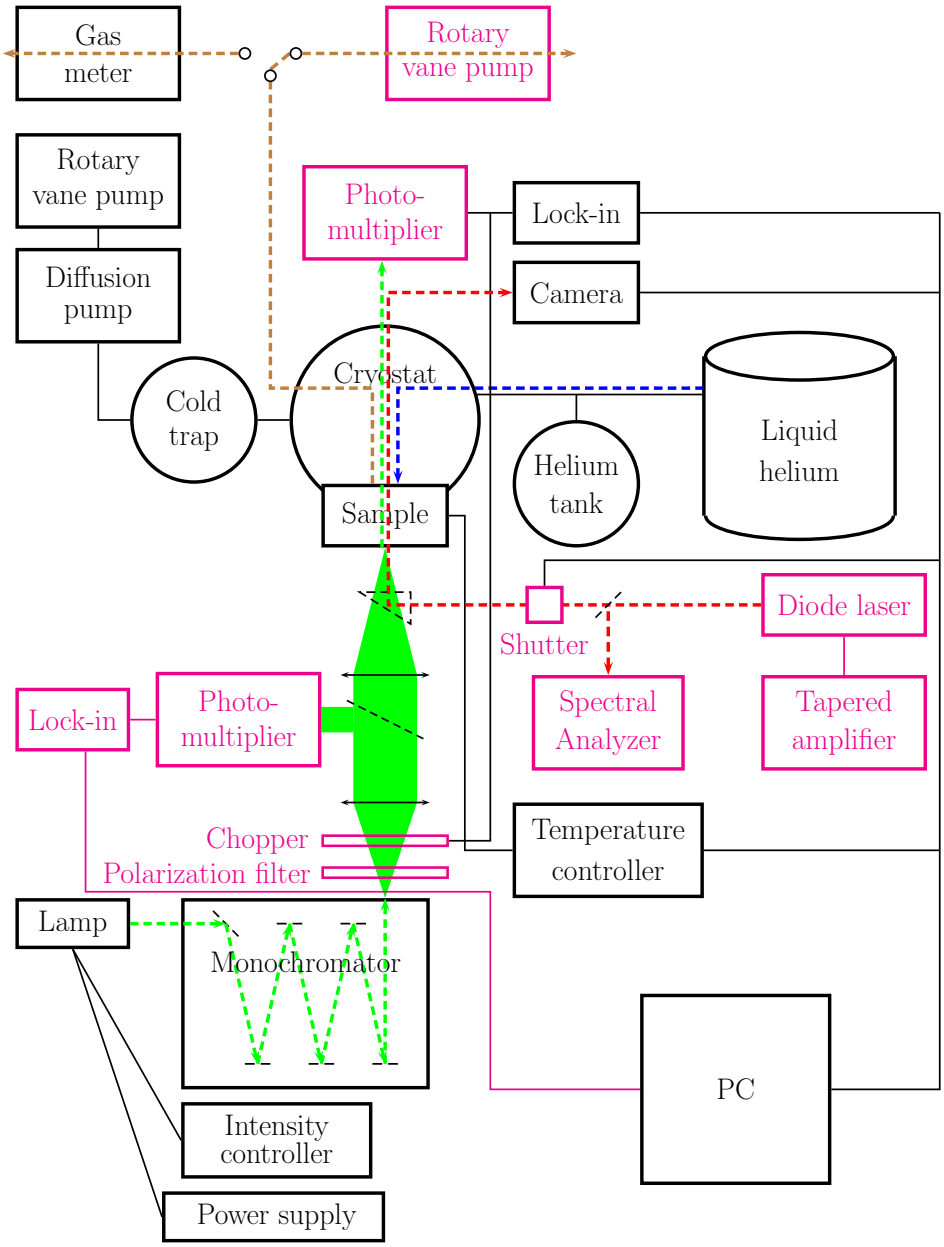

Figure 5.3: Illustrative scheme of the improved experimental set-up for spectral hole burning experiment in the absorption spectrum at LHe temperature. Green color indicates light from the wolfram lamp, red is the laser radiation, blue color depicts LHe and helium vapours are indicated by brown. Magenta color represents new components in the set-up (see section 5.5).

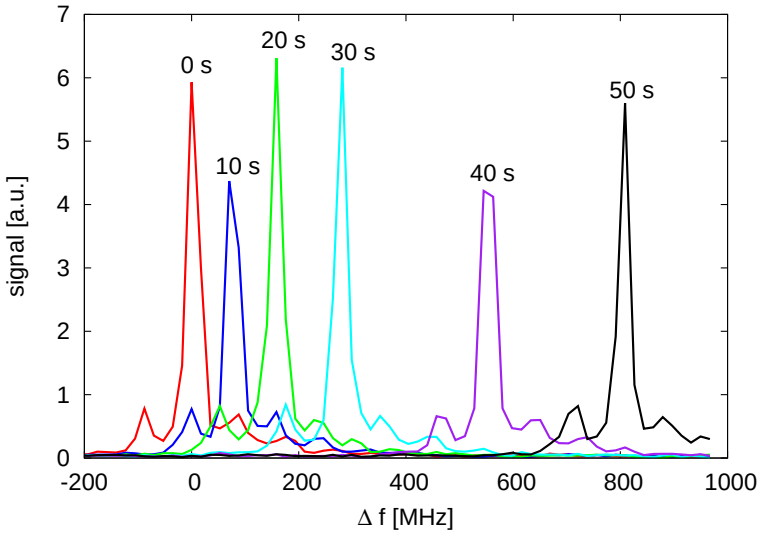

Figure 5.4: Frequency shift of the laser line in time due to temperature variations.

scanning of the single mode of the laser. Instead, the older concept of two-channel detection using original wolfram lamp as a light source together with monochromator was realized. Two-channel detection was used in order to eliminate lamp instability (see section 5.5.2).

5.5.2 Two-channel Detection

Two-channel detection enables to correct the absorption spectra in respect to a light source intensity used for linear spectrum measurements. The light is splitted into signal and reference channels after it had passed through a monochromator. The reference channel is directly focused to the photomultiplier while the light in signal channel enters the cryostat and after passing through the sample it is focused to the signal channel photomultiplier of the same type. The old photomultiplier RCA C31034 has been replaced by new Hamamatsu R943-02. Together with new photomultipliers, completely new collection optics for photomultipliers, water system for their cooling and a new light-tight cover of the whole set-up preventing parasite light from entering experimental set-up were developed, manufactured and installed (see figure 5.3).

Introducing two-channel detection mode uncovered two phenomenons which had to be dealt with. The first effect observed was spectrally different signal detected in the reference channel in comparison with signal channel while measured through an empty cryostat. The reason was that the monochromator gratings exhibit different reflectance for s and p polarization of light. Whereas p-polarized light is reflected on a beamsplitter more than s-polarized light (polarization by reflection), it gives rise to apparent absorption signal. This drawback was rectified by addition of near infrared (NIR) polarization filter CODIXX colorPol® VISIR CW02 just behind monochromator output slits (see figure 5.5).

Second phenomenon came to light in a form of interferences in the optical

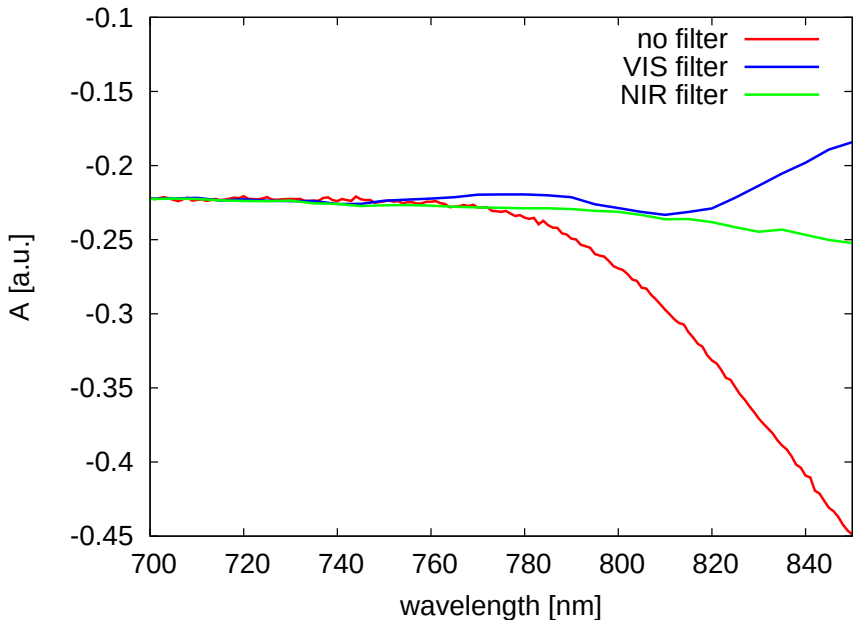

Figure 5.5: Comparison of detected absorption signal through an empty cryostat without any polarization filter (red), using visible polarization filter (blue) and using new NIR polarization filter CODIXX colorPol® VISIR CW02 (green). The offset of the line is due to unequal intensities in signal and reference channels.

system of unknown origin detected in both channels (see figure 5.6). All optical elements were investigated as potential sources of interferences and by excluding components one by one we came to the conclusion that the source is in the monochromator. However, we could not precisely determine the origin of the interferences. The interferences occur only when the step of the monochromator has been shorter than it was manufactured for (managed with unoriginal step motor) and forcing the monochromator beyond the construction limit can be the reason for interferences observation.

Because the origin of the interferences is in the monochromator they were present always in the past experiments (at least for 15 years) and only introducing two channel detection has revealed them. They used to be hidden in the noise and the experiments were conducted at shorter wavelengths where the interferences were not so strong. From the Fourier analysis it has been determined that the interferences consist of two main frequencies (see figure 5.7) which were then mathematically filtered out during the data evaluation.

5.5.3 Helium Vapours Pumping

Important parameter for any conducted experiment is S/N ratio in order to get the best possible results. One approach to improve the S/N ratio can be to increase the number of accumulations of the signal and to optimize the signal acquisition with the lock-in amplifiers. The limit of the hole burning experiment is that we need to acquire the best possible data within the shortest possible time in order to minimize the spontaneous hole filling (even when dealing with persistent holes). Lock-in amplifier parameters and the number of accumulations has been optimized but the main part of the noise was shown to originate in

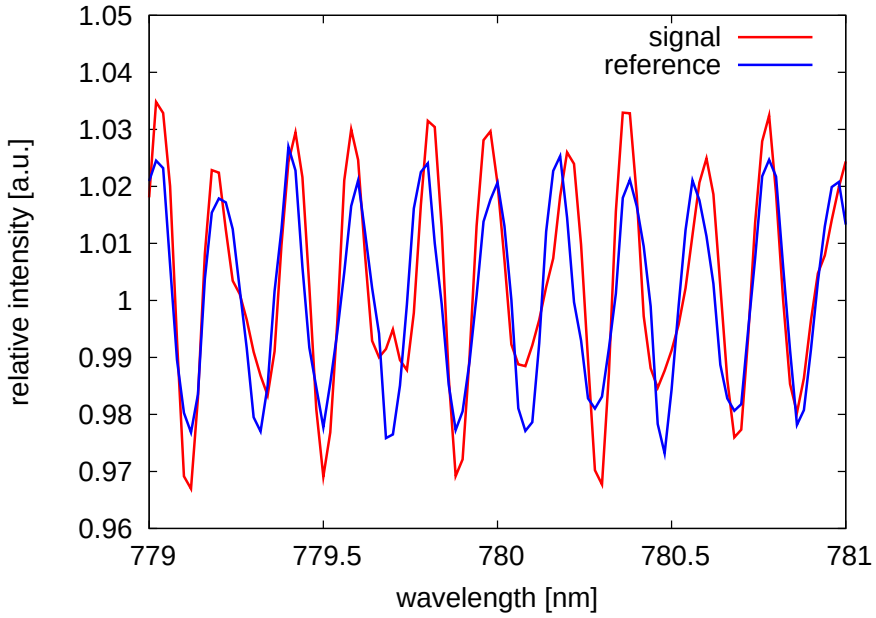

Figure 5.6: Relative intensities of interferences in signal and reference channels measured through an empty cryostat.

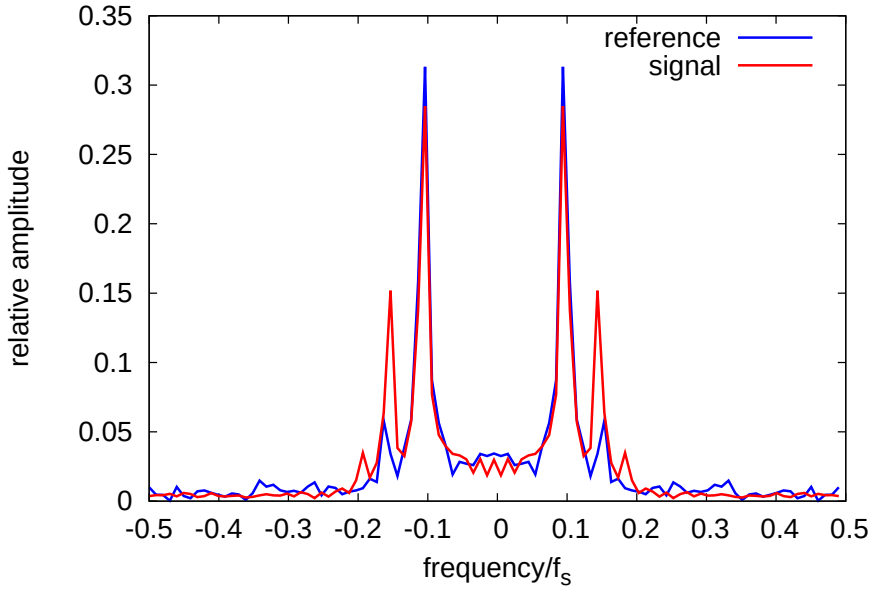

Figure 5.7: Fourier transformed spectra of the signal and reference channels measured through an empty cryostat (from figure 5.6). Frequencies of the interferences are relative to sampling frequency f_s (in our case is f_s determined by the step of the monochromator which was 0.02 nm). Frequency amplitudes are relative to the signal and reference channel amplitudes respectively.

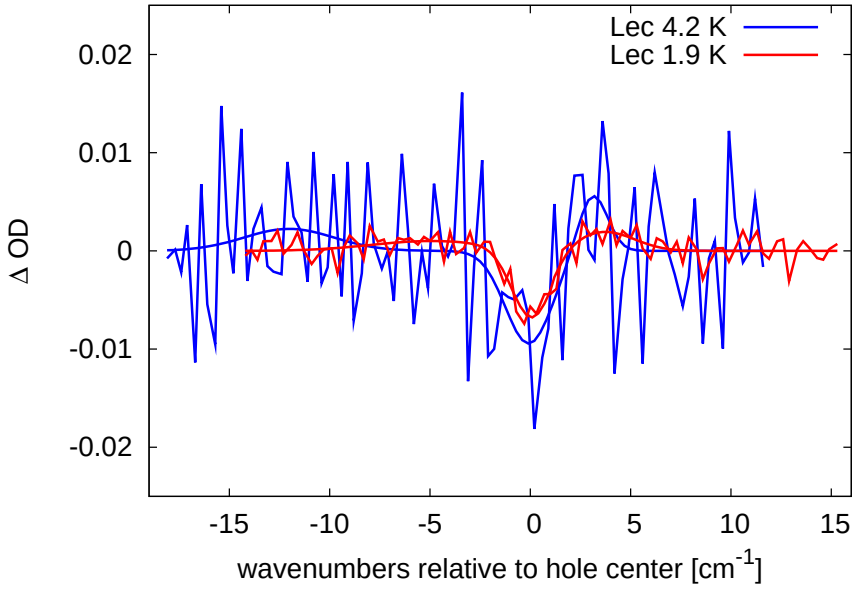

Figure 5.8: Effect of the helium vapours pumping on the hole burning spectrum for lecithin sample. Hole at 1.9 K (pumped) was burnt at 777.1 nm with burning dose 5.8 kJ·cm^{-2} and hole at 4.2 K (not pumped) was burnt at 775 nm with burning dose 33 kJ·cm^{-2}.

bubbles of the boiling helium during the experiment which diffract measuring light. To prevent helium in the sample space from boiling we decided to pump helium vapours from the sample tube, causing a pressure decrease which implicate lowering the boiling point of the helium. When the temperature gets as low as 2.17 K (for He-4), He undergoes the lambda point transition to superfluid state in which the thermal conductivity is extremely high. Therefore the heat normally causing boiling in the volume of the liquid is rapidly transferred to the surface where the boiling occurs at last (DRESNER, 2002). Helium pumping was realized by single stage rotary vane pump. The effect of measurement under the lambda point on hole spectrum is demonstrated in figure 5.8.

6. Materials

Samples studied in this work were artificial BChl *c* aggregates in aqueous solutions similar to chlorosomes of the green sulfur bacteria. The aim was to verify the role of quinones on the excitation quenching in the aggregates by comparison of aggregates with and without quinones. Apart from that it was proposed, that quinones should quench the excitation energy only in oxidized conditions. This phenomenon was investigated by adding sodium dithionite to the samples as a reducing agent. Aggregation of BChl *c* was induced either by lecithin or a quinone. BChl *c* was obtained by extraction from *Cba. tepidum* chlorosomes and by purification using high performance liquid chromatography (HPLC). Precise composition of the samples was as follows:

Quinone sample (*K2* sample) was prepared by mixing 20 µl 25 mM menaquinone-4 (vitamin K_2, Sigma, V9378) in ethanol with 25 µl 25 mM solution of BChl *c* in ethanol. This solution was injected vigorously into 1.25 ml Tris-HCL buffer of pH 8.0.

Lecithin sample (*Lec* sample) was prepared by mixing 20 µl 25 mM soy lecithin (95 % L-α-phosphatidyl choline, Avanti Polar Lipids) in ethanol with 25 µl 25 mM BChl *c* in ethanol. This solution was injected vigorously into 1.25 ml Tris-HCL buffer of pH 8.0.

These mixtures were retained for four days in the dark at room temperature for full aggregation. After that period 0.3 ml of each aggregate suspension was added to 0.4 ml glycerol. Mixture of water with glycerol ensures glassy matrix after freezing. Low temperature cuvettes were filled with these mixtures, which were subsequently slowly cooled down in the liquid nitrogen vapours while the glassy samples suitable for hole burning experiment were formed. Dithionite variants of the samples (*K2+dith* and *Lec+dith*) were made in completely the same way, but during the process of filling cuvettes 4.375 µl of 600 mM sodium dithionite was added to both samples resulting in sodium dithionite concentration of 14.6 mM.

7. Results

Experimental set-up was thoroughly discussed in chapter 5. Many improvements and modification of the experimental set-up with the aim of improving the S/N ratio and suppressing instrumental signal were introduced. Results of the improvements and difficulties connected with them are described and illustrated in section 5.5. Experimental results presented here are results on absorption spectroscopy of BChl *c* aggregates with different composition (see chapter 6) at room and liquid helium temperatures together with hole burning experiment on the aggregates as the pivotal theme of this master thesis.

7.1 Absorption Spectra

Absorption spectra at room and LHe temperatures were measured. Typical absorption spectra of all samples at both room and LHe temperatures are in the figures 7.1, 7.2, 7.3, and 7.4. Apart from that, comparison of all samples at room and LHe temperatures separately are in figures 7.5 and 7.6 respectively. In the case of *Lec* and *Lec+dith* samples there is a significant band at 670 nm from BChl *c* monomers which were proposed to be embedded in lecithin micelles (ALSTER et al., 2008). It is clear from the spectra that after cooling the sample down, the absorption significantly increase, the bands get narrower, moreover some of them undergo red shifts. Addition of dithionite has different effect on lecithin and quinone aggregates (figures 7.5 7.6, and chapter 8). Presence of dithionite in the samples was controlled by its absorption band around 320 nm at room temperature.

Red shifts were determined from the second derivatives of the original spectra. They are not the same for the different samples and some absorption bands do not shift at all. Up to 3 absorption bands were resolved. The main absorption bands maxima and Q_y band maxima values together with the red shifts due to the cooling are summarized in table 7.1. The red shifts are the same for the *K2* and *Lec* samples and their dithionite analogs respectively. The red-most absorption band is shifted by $\sim$5 nm in quinone samples which contrasts to $\sim$17 nm shift of the lecithin containing samples. The other maxima remain virtually at the same positions. As regards Q_y band maxima, they shift in the case of quinone samples by $\sim$2 nm and in the case of lecithin samples by $\sim$8 nm.

Further investigation of the temperature dependence of *Lec* and *K2* sample Q_y bands was made. Spectral shifts of the bands in temperature region of 1.9 – 100 K were determined from the second derivatives and the resulting dependence of spectral shifts on temperature is depicted in figure 7.7. All spectral bands resolved in Q_y band including whole Q_y band maxima positions remain unchanged. It illustrates that red shift occurs between room temperature and 100 K.

7.2 Hole Burning Experiment

Hole burning experiments were conducted on all samples in absorption spectrum. We obtained spectral holes at different wavelengths using different laser burning

Sample		Peak maxima [nm]		
		295 K	1.9 K	red shift
K2	1	767	772	**5**
	2	757	756	**-1**
	3	722	722	**0**
	Q_y	756	758	**2**
K2+dith.	1	768	774	**6**
	2	756	755	**-1**
	Q_y	759	761	**2**
Lec	1	751	768	**17**
	2	751	752	**1**
	Q_y	747	756	**9**
Lec+dith.	1	751	769	**18**
	2	751	753	**2**
	Q_y	747	756	**9**

Table 7.1: Absorption peaks maxima and Q_y band maximum together with their spectral shifts upon cooling. The experimental errors of the values are up to 1 nm.

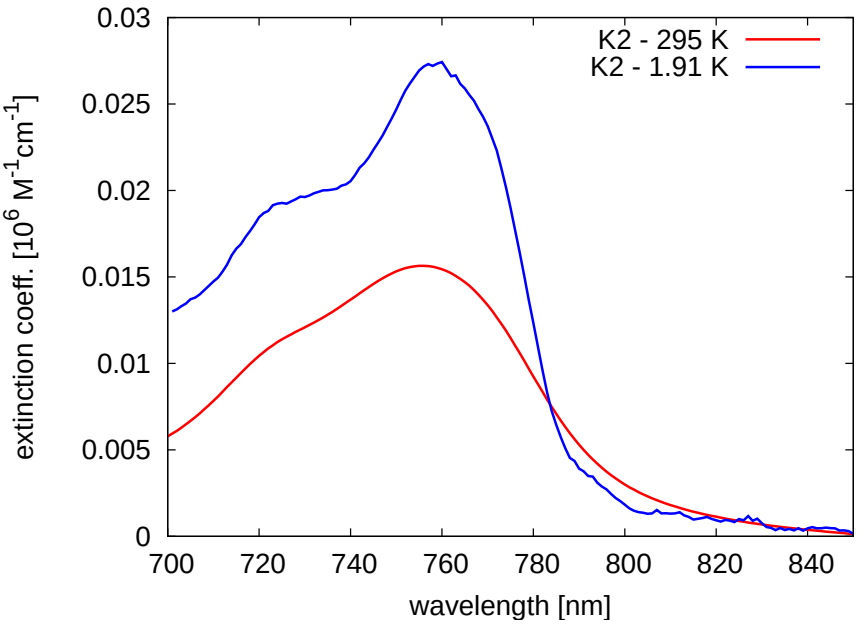

Figure 7.1: Comparison of *K2* sample absorption spectrum at room and low temperature.

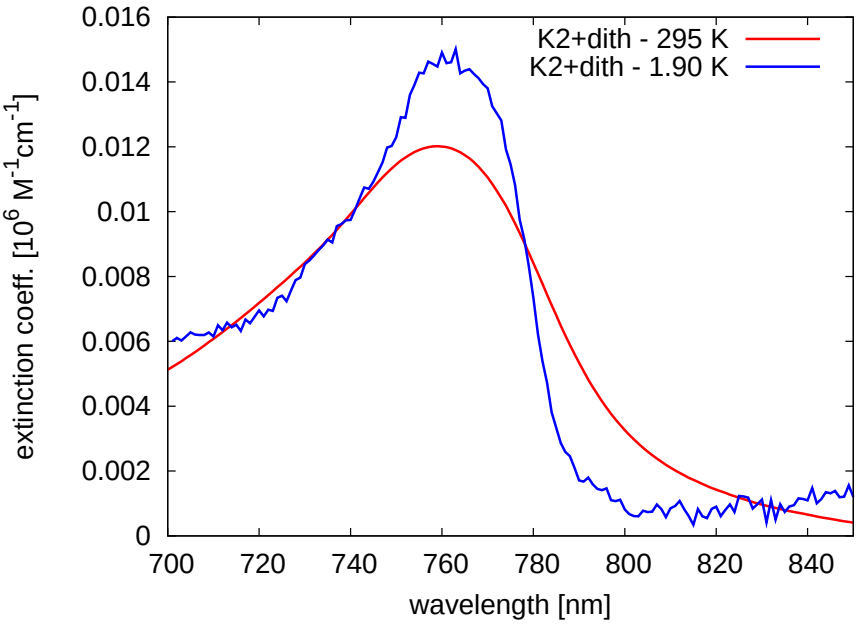

Figure 7.2: Comparison of *K2+dith* sample absorption spectrum at room and low temperature.

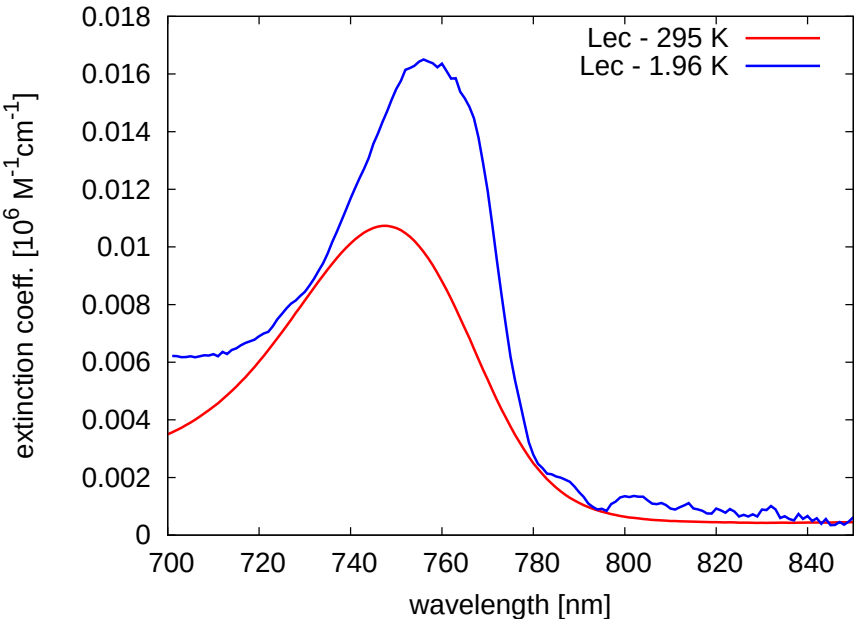

Figure 7.3: Comparison of *Lec* sample absorption spectrum at room and low temperature.

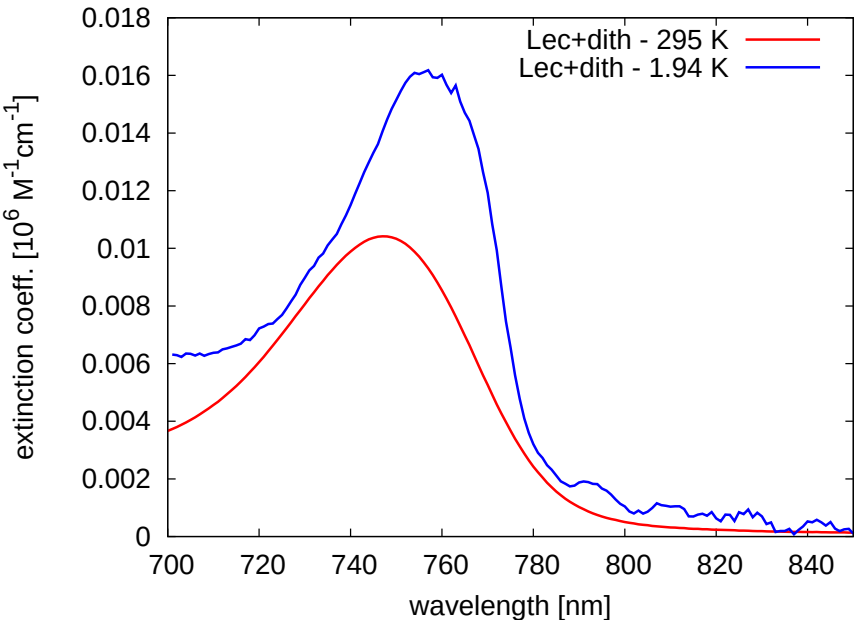

Figure 7.4: Comparison of *Lec+dith* sample absorption spectrum at room and low temperature.

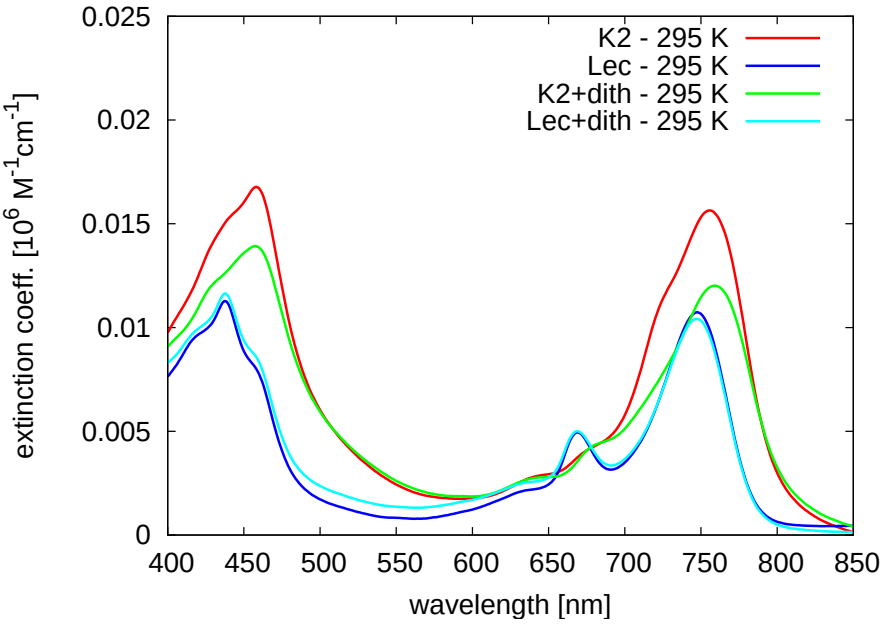

Figure 7.5: Absorption spectra of all the samples at room temperature.

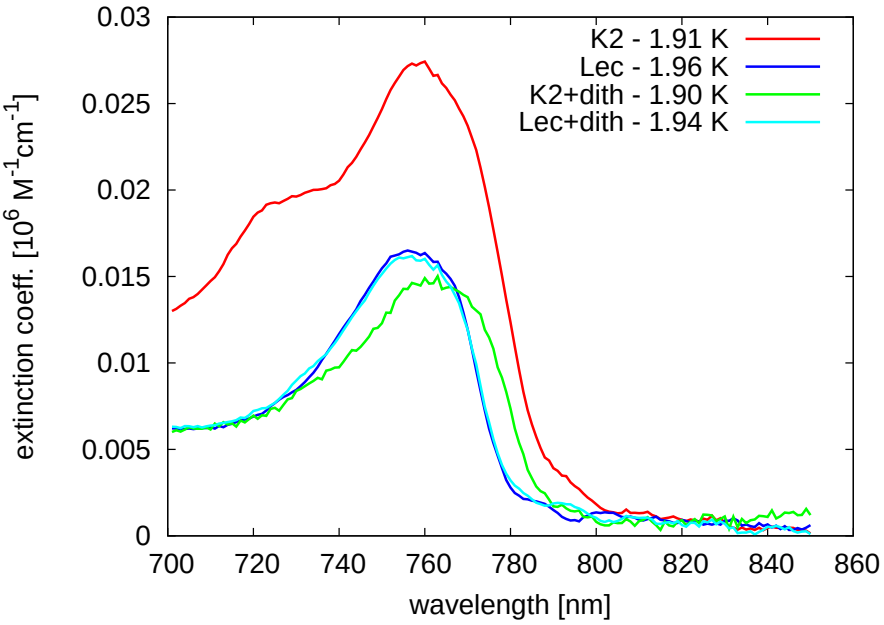

Figure 7.6: Absorption spectra of all the samples at low temperature.

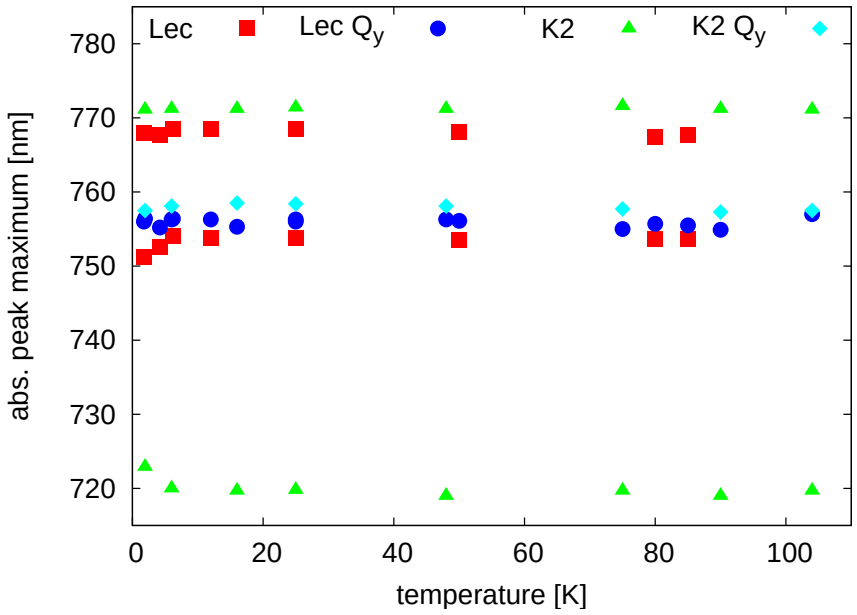

Figure 7.7: Temperature shifts of all absorption bands resolved in Q_y band including Q_y band maxima itself in the region between 1.9 – 100 K.

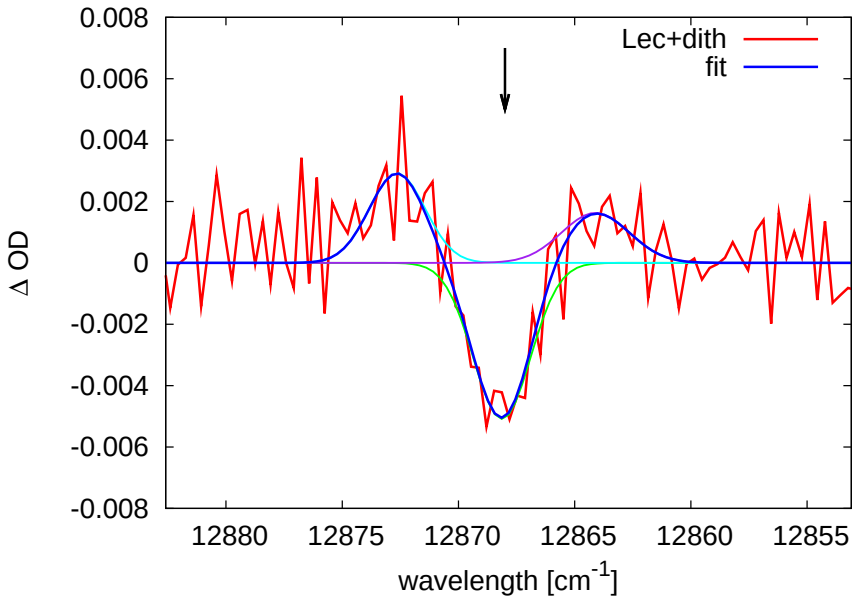

Figure 7.8: Typical spectral hole burnt in the absorption spectra of *Lec+dith* sample at 777.1 nm after burning dose 38.4 J·cm^{-2} using 2.5 mW laser power. The hole is fitted by 3 Gauss functions (green, cyan and purple) which resulted in final fit (blue). Burning wavelength is indicated by the arrow.

powers. At 777.1 nm we managed to burn holes in all samples which make possible to compare them. Observed spectral holes were resonant, mainly with antiholes on both sides of the holes. The holes were very shallow as the maximal relative depth was 5.2 % (see table 7.2). Due to a huge variety of hole shapes, hole widths were determined by different procedures from fitting by 2-3 Gauss functions with various initial and fitting parameters up to direct measurement of the hole width from the data without fitting. Typical hole burnt to the *Lec+dith* sample at 777.1 nm is depicted in figure 7.8.

Fluence dependencies obtained as a plot of hole width against the burning dose $P{\cdot}t/A$, where P is the laser power, t is burning time and A is the laser beam area were extrapolated to zero burning dose using all reasonable fit functions, specifically the function $\delta_{\mathrm{ZPL}} = \delta_{\mathrm{h}} + a(I\tau)^b$ with parameter b=0.25, b=0.5 (see section 4.3) and the linear function as the simplest option for cases in which the fluence dependence does not bend. From all these fits was chosen the most appropriate one which was then used for excited state lifetime calculation. Typical fluence dependence from *K2+dith* sample is showed in figure 7.9. For *Lec* and *K2* samples were obtained several fluence dependencies for different laser powers at 777.1 nm. All these fluences were used together to produce combined fluence for each of the samples. These combined fluences are depicted in figure 7.10 with corresponding detail in figure 7.11. Summary of the calculated excited state lifetimes is in table 7.3.

Temperature dependencies of the hole widths were investigated as well. However no temperature dependence was observed as can be seen in figure 7.12 for *Lec* sample. The experimental point at 4.2 K concisely illustrates influence of boiling helium on the experimental error as the rest of the data points are acquired under

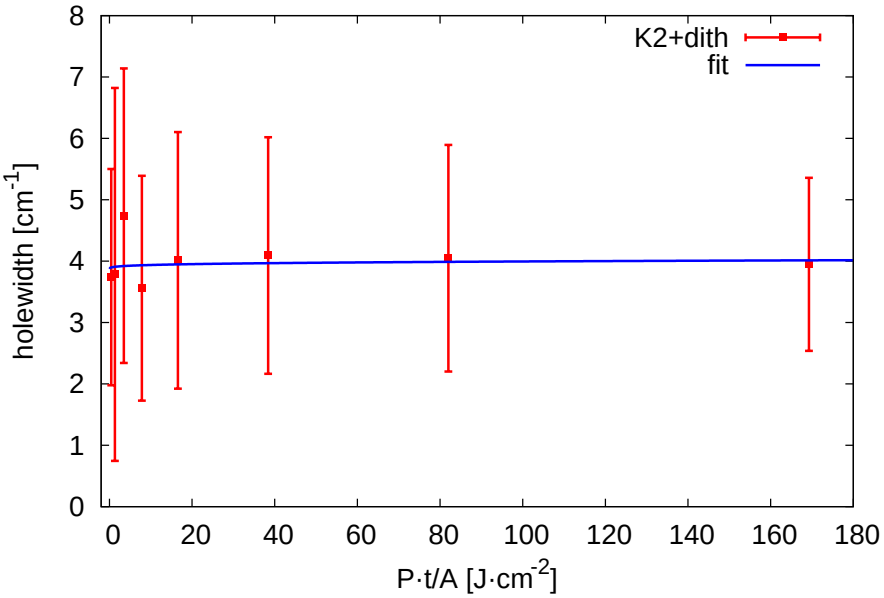

Figure 7.9: Fluence dependence of the *K2+dith* sample at 777.1 nm using 2.5 mW laser power. The fluence was fitted with function $\delta_{\mathrm{ZPL}} = \delta_{\mathrm{h}} + a(I\tau)^{0.25}$ via δ_{h} and a.

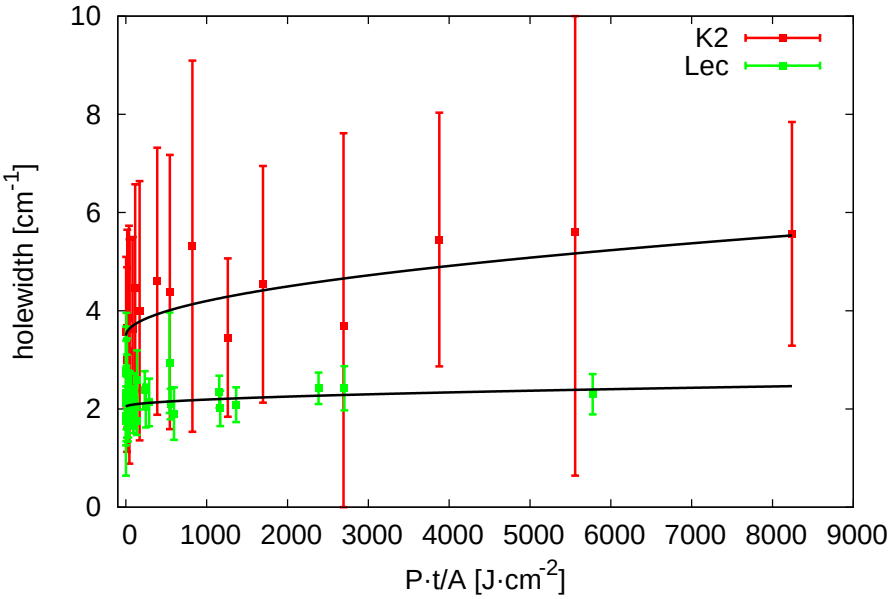

Figure 7.10: Combined fluence for *Lec* and *K2* samples at 777.1 nm with corresponding fit $\delta_{\mathrm{ZPL}} = \delta_{\mathrm{h}} + a(I\tau)^{0.5}$ via δ_{h} and a.

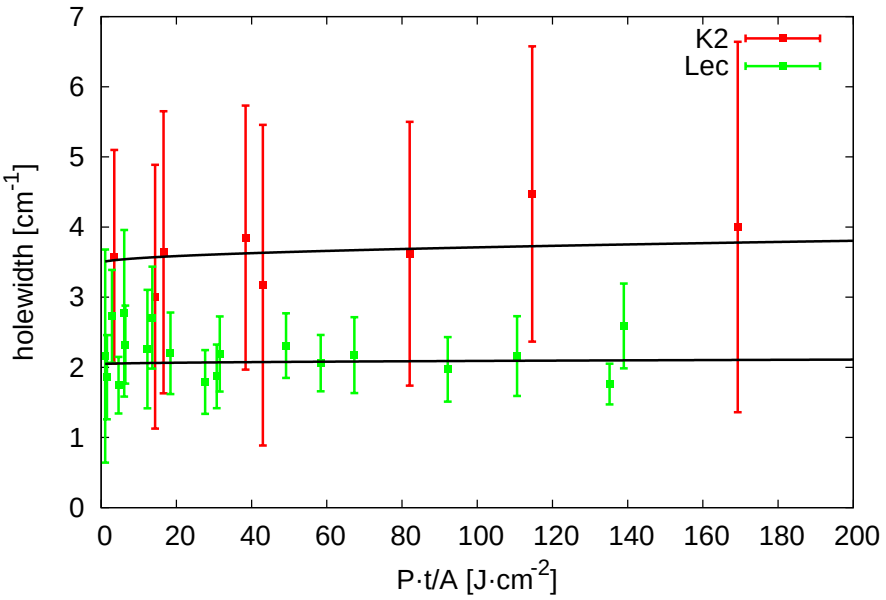

Figure 7.11: Detail of the combined fluence for *Lec* and *K2* samples at 777.1 nm with corresponding fit $\delta_{\mathrm{ZPL}} = \delta_{\mathrm{h}} + a(I\tau)^{0.5}$ via δ_{h} and a.

	Relative hole depth [%]			
Wavelength [nm]	K2	K2+dith.	Lec.	Lec+dith.
775			3.1	
777.1	0.5	3.2	2.1	5.2
780	0.8	4.0		
786	1.3			

Table 7.2: Comparison of relative hole depths for all the samples. Experimental errors of the values are up to ±0.5 %.

	Sample			
λ [nm]	K2 [ps]	K2+dith [ps]	Lec [ps]	Lec+dith [ps]
775			$3{,}29 \pm 0{,}13^{0.25}$*	
777,1	$3{,}04 \pm 0{,}15^{0.5}$	$2{,}75 \pm 0{,}20^{0.25}$	$5{,}19 \pm 0{,}17^{0.5}$	$3{,}73 \pm 0{,}06^{1}$
780	$3{,}36 \pm 0{,}24^{1}$	$5{,}29 \pm 0{,}83^{1}$		
786	$3{,}59 \pm 0{,}79^{1}$			

Table 7.3: Excited state lifetimes for all samples from hole burning experiment in absorption spectrum. Superscripts denotes the most appropriate fit, $^{0.25}$ and $^{0.5}$ refer to fits according to eq. 4.16 with b=0.25 and b=0.5 respectively. Superscript ^{1} refers to linear fit, * denotes values obtained without helium vapours pumping.

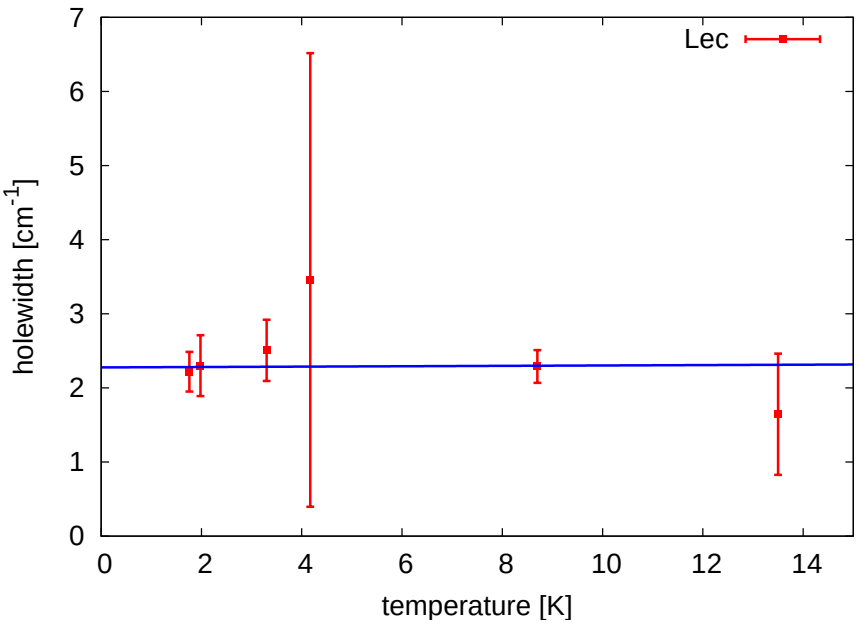

Figure 7.12: Temperature dependence of hole width for *Lec* sample at 777.1 nm in the region between 1.9 – 15 K.

superfluid or supercooled helium, and without helium at all. Since there is no temperature dependence in the region of 1.9 – 20 K, the pure dephasing time from eq. 4.14 can be neglected and it is plausible to calculate the excited state lifetime T_1 directly from eq. 4.15.

8. Discussion

Absorption spectra at room temperature are typical for lecithin aggregates (ALSTER et al., 2008) with peaks at 670 nm originating from BChl *c* monomers and maximum of the Q_y bands around 747 nm. On the contrary quinone aggregates undergoes extreme red shift of Q_y band up to 759 nm in the case of *K2+dith* sample due to BChl *c* aggregation. The red shift of the quinone samples has been always reported to be smaller (4 nm in (ALSTER et al., 2008)) than in lecithin aggregates based on the theory that quinones are present in between proposed lamellar system which causes smaller overlap integrals and therefore higher energy of the states. Lipids are bigger and are supposed to be outside the aggregates. Rest of the quinone aggregates not used for filling low temperature cuvettes did not precipitate on a bottom of an eppendorf tube and remain dense even after several months (lecithin aggregates precipitate in approximately two weeks). Together with high spectral shift these facts suggest high quality and big size of the quinone aggregates which can partially clarify the extreme spectral shift. Moreover, bigger size of the aggregates increases contribution of elastic scattering of the sample which shifts the absorption to the red as well. The sample preparation was the same as in previous publications investigating analogical aggregates (PALEČEK, 2009; ALSTER et al., 2008). Origin of the band peaking at 721 nm is still unknown, however it may correspond to some smaller oligomeric forms of BChl *c*.

As it can be seen in figures 7.5 and 7.6, dithionite has no effect on the *Lec* sample in contrast to *K2* sample where the addition of dithionite causes disappearance of the 721 nm band and significant absorption decrease of the whole Q_y band. It has probably structural significance. One possible interpretation is that dithionite in quinone sample can penetrate into the aggregates themselves in contrast to lecithin sample where the lipid layer keeps the dithionite outside the aggregate.

At least two spectral forms of BChl *c* were identified from the second derivatives of the BChl *c* aggregates spectra which is in agreement with previous results on chlorosomes (PŠENČÍK et al., 1998). Upon cooling of the samples down to 1.9 K one BChl *c* form undergo spectral red shift of 5 nm and 17 nm for *K2* and *Lec* samples respectively. Whole Q_y band absorption maximum shifts by 2 nm and 8 nm in *K2* and *Lec* samples respectively. Smaller red shift for quinone samples almost compensate the high red shift caused by aggregation in comparison to lecithin samples, but the Q_y band maxima are still somewhat red shifted (see table 7.1).

The lecithin samples data are in agreement with previous results and with published ones (ALSTER et al., 2008; PŠENČÍK et al., 1998). On the contrary extremely high red shift of quinone samples because of aggregation and subsequent low spectral shift due to the cooling has never been observed before even though composition of the samples is the same. Nonetheless absorption peaks behaviour is qualitatively in agreement with results published before for chlorosomes (PŠENČÍK et al., 1998) which indicates similarity between our aggregates and chlorosomal ones.

Absorption increase, narrowing of the bands and red shift observed at low

temperatures can be consistently elucidated by solvent effect as it contracts and it may also increase its polarity. These two factors can contribute to the absorption increase and red shift (DUDKOWIAK et al., 1995). This is supported by measurement of the temperature dependence between 1.9 – 100 K for *Lec* and *K2* samples which exhibit no changes in whole temperature region (see figure 7.7). Therefore, the red shift occurs at higher than 100 K temperatures, probably around the phase transition of a solvent. Smaller absorption increase in a case of *K2+dith* sample is most likely due to structural change as mentioned above.

In hole burning experiment, we managed to obtain only shallow holes: relative hole depths did not exceed 5 %. In the quinone sample holes were even more shallow which had negative effect on the experimental errors of the obtained hole widths as can be seen in figure 7.10. It was experimentally very difficult to identify and accurately evaluate such holes. For comparison, relative hole depths in comparable experiment conducted on chlorosomes in fluorescence spectra were up to 17 % (PŠENČÍK et al., 1994). Holes were fitted by Gauss functions rather than Lorentzian ones as the holes may be saturated in maximum and the burning process then follows only on hole edges, which widens the theory-accurate Lorentzian hole shape to the Gaussian one (so called fluence broadening). Only resonant ZPL with no phonon holes were observed similar to (PŠENČÍK et al., 1994). Antiholes present nearby the ZPL indicates nonphotochemical burning process.

Fluence dependencies were weakly dependent on burning dose and initial bending of the fluence dependencies were at the resolution limit which did not make possible to determine between dispersive and nondispersive burning kinetics. Only reliable information came from combined fluences (figure 7.10). Their fit parameters correspond rather to nondispersive characteristic.

Final excited state lifetimes obtained from hole burning experiments are summarized in table 7.3. These lifetimes are approximately 2 times longer than previously obtained results for analogous samples (PALEČEK, 2009). That can be partially clarified by using spectrally narrower laser by order of magnitude, improvement of S/N ratio which made possible to resolve shallower holes and detect holes using lower burning doses. This implicates better approximation of the fluence at the beginning with using fit according to eq. (4.16) which results in narrower holes that give longer lifetimes.

Comparing the excited state lifetimes obtained at the same wavelength of 777.1 nm, it is clear that quinone plays significant role in excitation quenching at aerobic conditions (FRIGAARD et al., 1997) as the lifetime shortens by $\sim$2 ps. That is supported by the fact that holes in quinone samples were more shallow and it was far more difficult to obtain them which indicates that the excited states are quenched rapidly because the burning efficiency is low. According to the theory and results obtained on chlorosomes (PŠENČÍK et al., 1994), addition of sodium dithionite induces anaerobic conditions under which quinone does not quench the excitation and the lifetimes should prolong to the level of *Lec* sample (ALSTER et al., 2008). We observed totally different behaviour as the added dithionite caused more pronounced quenching than without it. Moreover, relative hole depths in dithionite samples increased (see table 7.2). These facts support an idea that dithionite cause some structural change in the aggregates which is in the case of *K2+dith* sample indicated by the linear absorption as well because of

change in a blue part of the Q_y band (disappearance of 720 nm band and decrease of absorption). *Lec+dith* sample shows the highest burning efficiency (see table 7.2). The resulting fluence dependence was only possible to fit with linear function (see table 7.3). These facts indicate that 2.5 mW burning power used as the lowest one during all experiments was still not low enough for *Lec+dith* sample to get good approximation of the beginning of the fluence. This could induce maximally 0.5 ps difference but it is still not enough to clarify such discrepancy in excited state lifetimes between *Lec* and *Lec+dith* samples. On the other side, linear absorption spectrum does not change upon addition of dithionite in the case of lecithin sample (see figures 7.5 and 7.6). All these facts suggest that the change caused in BChl *c* aggregates upon dithionite addition may have different structural evidence due to different aggregation inducing agent. However, the effect of the structural change on excitation quenching is the same (see tables 7.3 and 7.2).

Significant change occurs at 780 nm where the behaviour of quinone sample seems to follow the theory upon addition of dithionite as the excited state lifetime prolong to the level of *Lec* sample. That could mean that the dithionite-induced change in aggregates influence only some energetic states in the aggregate. For confirmation of such statement, it would be useful to obtain data for more wavelengths in a form of ZPL action spectra (dependence of relative hole depths on the burning wavelength for constant burning dose) to reveal the distributions of the lowest excited states as the samples do have absorption edge on different wavelengths. Excited state lifetime determined from hole burning experiment on chlorosomes was 2.7 ps at 780 nm in absorption (PŠENČÍK et al., 1998). Value obtained at the same wavelength for BChl *c* aggregates was 3.4 ps which follows the fact that natural chlorosome systems are quenching the excitation energy more efficiently than BChl *c* aggregates despite $\sim$10 times higher quinone concentration in comparison to chlorosomes (FRIGAARD – BRYANT, 2006).

The excited state lifetimes prolong with increasing wavelength for all samples which is caused by the quenching of the shorter wavelength states by those of longer wavelength and it is similar to chlorosomes. All samples show no temperature dependencies in the region of 1.9 – 20 K similarly to experiments on chlorosomes in absorption (PŠENČÍK et al., 1998) and fluorescence as well (PŠENČÍK et al., 1994).

9. Summary

Significant improvement of an original experimental set-up has been achieved. Experiment results were therefore obtained with $\sim$6 times higher S/N ratio and with better suppressed instrumental signal and parasite light compared to the original experimental set-up. New diode laser provided better power stability and greater variety of burning powers and available wavelengths. Two channel detection enabled to correct the absorption spectra in respect to the light source intensity. It helped to discover the interferences originating in monochromator as well. Helium vapours pumping prevent helium from boiling in sample space which provided $\sim$6 times higher S/N ratio during hole burning experiment.

Absorption spectra show similarities of artificial aggregates to chlorosomes at both room and low temperatures. At least two spectral forms of BChl *c* were resolved from the linear absorption spectra of the aggregates. Hole burning experiments in absorption spectra confirm the role of quinones (explicitly menaquinone-4) in excitation quenching in the aggregates under aerobic conditions. Spectral holes burnt in the red part of Q_y band of BChl *c* aggregates were shallow, resonant and with nonphotochemical products. Hole burning efficiency was higher for *Lec* samples (relative hole depth $\sim 3\,\%$) in contrast to *K2* sample with relative hole depth of $\sim 1\,\%$. Significant increase of burning efficiency upon addition of sodium dithionite in both samples were observed. Excited state lifetime shortened from $\sim$5 ps for *Lec* sample to $\sim$3 ps for *K2* sample at 777.1 nm. Under anaerobic conditions (after addition of sodium dithionite) we observed more pronounced quenching of excitation energy that we attribute to the structural change induced by dithionite which probably gets into the self-assembled bacteriochlorophylls. It does not seem to be the case for all wavelengths but this hypothesis need to be confirmed by additional data for more wavelengths. No temperature dependencies were observed for all the samples.

Bibliography

ALSTER, J. et al. Effects of quinones on formation and properties of bacteriochlorophyll aggregates. *Photosynth. Res.* 2008, 95, p. 183–189.

ARELLANO, J. B. et al. Effect of carotenoid deficiency on cells and chlorosomes of *Chlorobium phaeobacteroides*. *Archives of Microbiology*. 2001, 175, p. 226–233.

ASAO, M. – MADIGAN, M. T. Taxonomy, phylogeny, and ecology of the heliobacteria. *Photosynthesis Research*. 2010, 104, p. 103–111.

BALABAN, T. S. Tailoring Porphyrins and Chlorins for Self-Assembly in Biomimetic Artificial Antenna Systems. *Acc. Chem. Res.* 2005, 38, p. 612–623.

BEATTY, J. T. et al. An obligately photosynthetic bacterial anaerobe from a deep-sea hydrothermal vent. *PNAS*. 2005, 102, p. 9306–9310.

BLANKENSHIP, R. E. et al. Redox regulation of energy transfer efficiency in antennas of green photosynthetic bacteria. *Photochem Photobiol*. 1993, 57, p. 103–107.

BLANKENSHIP, R. E. *Molecular Mechanisms of Photosynthesis*, volume 1, Photosynthetic Organisms and Organelles, p. 11–25. Blakwell Science Ltd, London, 2002. ISBN 0-632-04321-0.

BLANKESHIP, R. E. – OLSON, J. M. – MILLER, M. *Anoxygenic Photosynthetic Bacteria*, volume 2, Antenna Complexes from Green Photosynthetic Bacteria, p. 399–435. Kluwer Academic Publishers, Dordrecht, 1995. ISBN 0-306-47954-0.

BORREGO, C. M. et al. Light intensity effects on pigment composition and organisation in the green sulfur bacterium *Chlorobium tepidum*. *Photosynthesis Research*. 1999, 59, p. 159–166.

BROCKMANN, H. – LIPINSKI, A. Bacteriochlorophyll *g*. A new bacteriochlorophyll from *Heliobacterium chlorum*. *Archives of Microbiology*. 1983, 136, number 1, p. 17–19.

BRUNE, D. C. et al. Antenna Organization in Green Photosynthetic Bacteria. 2. Excitation Transfer in Detached and Membrane-Bound Chlorosomes from *Chloroflexus aurantiacus*. *Biochemistry*. 1987a, 26, p. 8652–8658.

BRUNE, D. C. et al. Antenna Organization in Green Photosynthetic Bacteria. 1. Oligomeric Bacteriochlorophyll c as a Model for the 740 nm Absorbing Bacteriochlorophyll c in Chloroflexus aurantiacus Chlorosomes. *Biochemistry*. 1987b, 26, p. 8644–8652.

BRYANT, D. A. et al. Selective Protein Extraction from *Chlorobium tepidum* Chlorosomes Using Detergents. Evidence That CsmA Forms Multimers and Binds Bacteriochlorophyll *a*. *Biochemistry*. 2002, 41, p. 14403–14411.

CAMARA-ARTIGAS, A. – BLANKENSHIP, R. E. – ALLEN, J. P. The structure of the FMO protein from *Chlorobium tepidum* at 2.2 Å resolution. *Photosynthesis Research*. 2003, 75, p. 49–55.

CARBONERA, D. et al. Fluorescence and Absorption Detected Magnetic Resonance of Membranes from the Green Sulfur Bacterium *Chlorobium limicola*. Full Assignment of Detected Triplet States. *J. Phys. Chem. B*. 2002, 106, p. 7560–7568.

CHUNG, S. et al. Genes encoding two chlorosome components from the green sulfur bacteria *Chlorobium vibrioforme* strain 8327D and *Chlorobium tepidum*. *Photosynthesis Research*. 1994, 41, p. 261–275.

DAVYDOV, A. S. *Kvantová Mechanika*. volume 1. Praha : SPN, 1978. Přeložil Luboš Valenta et al.; Ilustrace Josef Kubík. ISBN 3-540-18607-7.

DRESNER, L. *Stability of Superconductors*, volume, Cooling with Superfluid Helium, p. 175–184. Kluwer Academic Publishers, 2002. ISBN 0-306-47064-0.

DUDKOWIAK, A. – FRANCKE, C. – AMESZ, J. Aggregation of 8,12-diethyl farnesyl bacteriochlorophyll *c* at low temperature. *Photosynthesis research*. 1995, 46, number 3, p. 427–433.

DĚDIC, R. *Spectroscopic Study of Photosystem II Reaction Center*. PhD thesis, Universitas Carolina Pragensis, Facultas Mathematica Physicaque, Department of Chemical Physics and Optics, Prague, 2000.

EMERSON, R. – ARNOLD, W. The Photochemical Reaction in Photosynthesis. *The Journal of General Physiology*. 1932, 16, p. 191–205.

FASSIOLI, F. – NAZIR, A. – OLAYA-CASTRO, A. Quantum State Tuning of Energy Transfer in a Correlated Environment. *J. Phys. Chem. Lett.* 2010, 14, number 1, p. 2139–2143.

FEICK, R. G. – FULLER, R. C. Topography of the Photosynthetic Apparatus of *Chloroflexus aurantiacus*. *Biochemistry*. 1984, 23, p. 3693–3700.

FRIDRICH, J. – HAARER, D. Photochemical Hole Burning: A Spectroscopic Study of Relaxation Processes in Polymers and Glasses. *Angewante Chemie*. 1984, 23, number 2, p. 113–140.

FRIGAARD, N.-U. – BRYANT, D. A. *Complex Intracellular Structures in Prokaryotes*, volume 2 / *Microbiology Monographs*, Chlorosomes: Antenna Organelles in Photosynthetic Green Bacteria, p. 79–114. Springer-Verlag Berlin Heidelberg, 2006. ISBN 978-3-540-32524-6.

FRIGAARD, N.-U. et al. Quinones in chlorosomes of green sulfur bacteria and their role in redox-dependent fluorescence studied in chlorosome-like bacteriochlorophyll *c* aggregates. *Arch Microbiol*. 1997, 167, number 2, p. 343–349.

FRIGAARD, N.-U. et al. Studies of the location and function of isoprenoid quinones in chlorosomes from green sulfur bacteria. *Photosynthesis Research*. 1998, 58, p. 81–90.

FRIGAARD, N.-U. et al. Diastereoselective Control of Bacteriochlorophyll *e* Aggregation. 31-S-BChl *e* Is Essential for the Formation of Chlorosome-Like Aggregates. *J. Phys. Chem. B.* 2000, 104, p. 10379–10386.

FRIGAARD, N.-U. et al. Isolation and characterization of carotenosomes from a bacteriochlorophyll c-less mutant of Chlorobium tepidum. *Photosynthesis Research.* 2005, 86, number 2–3, p. 101–111.

GANAPATHY, S. et al. Alternating syn-anti bacteriochlorophylls form concentric helical nanotubes in chlorosomes. *PNAS.* 2009, 106, p. 8525–8530.

GEMERDEN, H. V. – MAS, J. *Anoxygenic Photosynthetic Bacteria*, volume 2, Ecology of Phototrophic Sulfur Bacteria, p. 50–79. Kluwer Academic Publishers, Dordrecht, 1995. ISBN 0-306-47954-0.

GEST, H. – FAVINGER, J. L. *Heliobacterium chlorum*, an anoxygenic brownish-green photosynthetic bacterium containing a "new" form of bacteriochlorophyll. *Archives of Microbiology.* 1983, 136, number 1, p. 11–16.

GEST, H. – PIETRO, A. S. – VERNON, L. P. (Ed.). *Bacterial photosynthesis*, volume 1, Yellow Springs, Ohio, 1963. Antioch Press.

GOROKHOVSKII, A. – KAARLI, R. – REBANE, L. Hole burning in the contour of a pure electronic line in Shpolskii system. *JETP Lett.* 1974, 20, p. 216–220.

HANADA, S. – PIERSON, B. *The Prokaryotes*, volume 7, The Family Chloroflexaceae, p. 815–842. Springer Science+Bussiness Media,LLC, Berlin, 2006. ISBN 0-387-25497-8.

HIROTA, M. et al. The effect of detergent on the structure and composition of chlorosomes isolated from *Cf. aurantiacus*. *Biochim Biophys Acta.* 1992, 1099, p. 271–274.

HOLZWARTH, A. R. – SCHAFFNER, K. On the structure of bacteriochlorophyll molecular aggregates in the chlorosomes of green bacteria. A molecular modelling study. *Photosynthesis Research.* 1994, 41, p. 225–233.

HUSTER, M. S. – SMITH, K. M. Biosynthetic Studies of Substituent Homologation in Bacteriochlorophylls *c* and *d*. *Biochemistry.* 1990, 29, p. 4348–4355.

IMHOFF, J. F. *Anoxygenic Photosynthetic Bacteria*, volume 2, Taxonomy and Physiology of Phototrophic Purple Bacteria and Green Sulfur Bacteria, p. 1–15. Kluwer Academic Publishers, Dordrecht, 1995. ISBN 0-306-47954-0.

KAMPF, C. – PFENNING, N. Capacity of chromatiaceae for chemotrophic growth. Specific respiration rates of *Thiocystis violacea* and *Chromatium vinosum*. *Archives of Microbiology.* 1980, 127, number 2, p. 125–135.

KHARLAMOV, B. M. – PERSONOV, R. – BYKOVSKAYA, L. Stable 'gap' in absorption spectra of solid solutions of organic molecules by laser irradiation. *Optics Communications.* 1974, 12, p. 191–193.

KIMBLE-LONG, L. K. – MADIGAN, M. T. Molecular evidence that the capacity for endosporulation is universal among phototrophic heliobacteria. *FEMS Microbiology Letters*. 2001, 199, p. 191–195.

KLINGER, P. et al. Effects of Carotenoids and Monogalactosyl Diclyceride on Bacteriochlorophyll *c* Aggregates in Aqueous Buffer: Implications for the Self-assembly of Chlorosomes. *Photochemistry and Photobiology*. 2004, 80, p. 572–578.

KRASNOVSKY, A. – BYSTROVA, M. Self-assembly of chlorophyll aggregated structures. *BioSystems*. 1980, 12, p. 181–194.

LI, H. et al. Molecular Contacts for Chlorosome Envelope Proteins Revealed by Cross-Linking Studies with Chlorosomes from *Chlorobium tepidum*. *Biochemistry*. 2006, 45, p. 9095–9103.

MADIGAN, M. T. – JUNG, D. O. *The Purple Phototrophic Bacteria*, volume 28 / *Advances in Photosynthesis and Respiration*, An Overview of Purple Bacteria: Systematics, Physiology, and Habitats, p. 1–15. Springer Science+Bussiness Media BV, Dordrecht, 2008. ISBN 978-1-4020-8815-5.

MATSUURA, K. et al. Spectral forms and orientation of bacteriochlorophylls *c* and *a* in chlorosomes of the green photosynthetic bacterium *Chloroflexus aurantiacus*. *Photochemistry and Photobiology*. 1993, 57, p. 92–97.

MELØ, T. et al. Electronic energy transfer involving carotenoid pigments in chlorosomes of two green bacteria: *Chlorobium tepidum* and *Chloroflexus aurantiacus*. *Spectrochimica Acta Part A*. 2000, 56, p. 2001–2010.

MILLER, K. R. et al. *Heliobacterium chlorum*: cell organization and structure. *Archives of Microbiology*. 1986, 140, number 2, p. 111–114.

MILLER, M. – SIMPSON, D. – REDLINGER, T. High degree of organization of bacteriochlorophyll *c* in chlorosome-like aggregates spontaneously assembled in aqueous solution. *Photosynthesis Research*. 1993, 35, p. 275–283.

MOERNER, W. (Ed.). *Topics in Current Physics: Persistent Spectral Hole-Burning: Science and Applications*, volume, Introduction, Basic Principles and Methods of Persistent Spectral Hole-Burning, p. 1–79. Springer-Verlag Berlin Heidelberg, Berlin, 1988. ISBN 3-540-18607-7.

MONTANO, G. A. et al. Characterization of *Chlorobium tepidum* Chlorosomes: A Calculation of Bacteriochlorophyll *c* per Chlorosome and Oligomer Modeling. *Biophysical Journal*. 2003, 85, p. 2560–2565.

NOZAWA, T. et al. Structures of chlorosomes and aggregated BChl *c* in *Chlorobium tepidum* from solid state high resolution CP/MAS ^{13}C NMR. *Photosynthesis Research*. 1994, 41, p. 211–223.

OELZE, J. – GOLECKI, J. R. *Anoxygenic Photosynthetic Bacteria*, volume 2, Membranes and Chlorosomes of Green Bacteria: Structure, Composition and Development, p. 259–278. Kluwer Academic Publishers, Dordrecht, 1995. ISBN 0-306-47954-0.

OLSON, J. – J.P.PEDERSEN. Bacteriochlorophyll *c* momomers, dimers, and higher aggregates in dichloromethane, chloroform, and carbon tetrachloride. *Photosynthesis Research*. 1990, 25, p. 25–37.

PALEČEK, D. : Excitation Quenching in Bacteriochlorophyll Aggregates. Bachelor's thesis, 2009. in czech.

PŠENČÍK, J. et al. Hole burning study of excited state structure and energy transfer dynamics of bacteriochlorophyll *c* in chlorosomes of green sulphur photosynthetic bacteria. *Photosynthesis Research*. 1994, 42, p. 1–8.

PŠENČÍK, J. et al. Fast energy transfer and exciton dynamics in chlorosomes of the green sulphur bacterium *Chlorobium tepidum*. *Journal Phys. Chem. A*. 1998, 102, p. 4392–4398.

PŠENČÍK, J. et al. Lamellar Organization of Pigments in Chlorosomes, the Light Harvesting Complexes of Green Photosynthetic Bacteria. *Biophysical Journal*. 2004, 87, p. 1165–1172.

PŠENČÍK, J. et al. Internal Structure of Chlorosomes from Brown-Colored Chlorobium Species and the Role of Carotenoids in Their Assembly. *Biophysical Journal*. 2006, 91, p. 1433–1440.

PŠENČÍK, J. et al. The lamellar spacing in self-assembling bacteriochlorophyll aggregates is proportional to the length of the esterifying alcohol. *Photosynthesis Research*. 2010, 104, p. 211–219.

RAJA, N. – REDDY, S. – SMALL, G. *Biophysical Techniques in Photosynthesis*, volume, Spectral Hole Burning: Methods and Applications to Photosynthesis, p. 123–136. Kluwer Academic Publishers, 1996.

SMITH, K. M. – KEHRES, L. A. Aggregation of the Bacteriochlorophylls *c*, *d*, and *e*. Models for the Antenna Chlorophylls of Green and Brown Photosynthetic Bacteria. *J. Am. Chem. Soc.* 1983, 105, p. 1387–1389.

SØRENSEN, P. G. – COX, R. P. – MILLER, M. Chlorosome lipids from *Chlorobium tepidum*: characterization and quantification of polar lipids and wax esters. *Photosynthesis Research*. 2008, 95, number 2–3, p. 191–196.

STACKEBRANDT, E. – RAINEY, F. A. – WARD-RAINEY, N. Anoxygenic phototrophy across the phylogenetic spectrum: current understanding and future perspectives. *Archives of Microbiology*. 1996, 166, number 4, p. 211–223.

SUNDSTRÖM, V. – GRONDELLE, R. *Anoxygenic Photosynthetic Bacteria*, volume 2, Kinetics of Excitation Transfer and Trapping in Purple Bacteria, p. 349–372. Kluwer Academic Publishers, Dordrecht, 1995. ISBN 0-306-47954-0.

TAKAICHI, S. *The Photochemistry of Carotenoids*, volume 8 / *Advances in Photosynthesis and Respiration*, Carotenoids and Carotenogenesis in Anoxygenic Photosynthetic Bacteria, p. 39–69. Kluwer Academic Publishers, Dordrecht, 2004. ISBN 0-306-48209-6.

TÖRNROTH-HORSEFIELD, S. – NEUTZE, R. Opening and closing the metabolite gate. *Biochemistry and Biophysics*. 2008, 105, number 50, p. 19565–19566.

TRANTER, G. – HOLMES, J. – LINDON, J. (Ed.). *Encyclopedia of Spectroscopy and Spectrometry, Part I*, volume, Hole Burning Spectroscopy, Methods, p. 826–836. Academic Press, 2000. ISBN 0-12-226680-3.

UEHARA, K. – OLSON, J. Bacteriochlorophyll *c* momomers, dimers, and higher aggregates in dichloromethane, chloroform, and carbon tetrachloride. *Photosynthesis Research*. 1992, 33, p. 251–257.

VANNOORT, P. et al. Redox Effects on the Excited-State Lifetime in Chlorosomes and Bacteriochlorophyll c Oligomers. *Biophysical Journal*. 1997, 72, p. 316–325.

WANG, J. – BRUNE, D. C. – BLANKENSHIP, R. E. Effects of oxidants and reductants on the efficiency of excitation transfer in green photosynthetic bacteria. *Biochimica et Biophysica Acta*. 1990, 1015, p. 457–463.

WOESE, C. R. – FOX, G. E. Phylogenetic structure of the prokaryotic domain: The primary kingdoms. *PNAS*. 1977, 74, number 11, p. 5088–5090.

WOESE, C. R. et al. Conservation of primary structure in 16S ribosomal RNA. *Nature*. 1975, 254, number 1, p. 83–86.

XIN, Y. et al. Purification and Characterization of the B808–866 Light-harvesting Complex from Green Filamentous Bacterium *Chloroflexus aurantiacus*. *Photosynthesis Research*. 2005, 86, number 1-2, p. 155–163.

List of Tables

List of Figures